The GTPase Nog1 co-ordinates assembly, maturation and quality control of distant ribosomal functional centers

Purnima Klingauf-Nerurkar[1,6], Ludovic Gillet[2,6], Daniela Portugal-Calisto[1], Michaela Oplova[1,3], Martin Jäger[3], Olga T. Schubert[2,4], Agnese Pisano[1], Cohue Peña[1], Sanjana Rao[1], Martin Altvater[3], Yiming Chang[3], Ruedi Aebersold[2,5] & Vikram Govind Panse[1]*

[1]Institute of Medical Microbiology, University of Zurich, CH-8006 Zurich, Switzerland

[2]Institute of Molecular Systems Biology, ETH Zurich, CH-8093 Zurich, Switzerland

[3]Institute of Biochemistry, ETH Zurich, CH-8093 Zurich, Switzerland

[4]Current address: Department of Human Genetics, University of California, Los Angeles, Los Angeles, CA 90095, USA

[5]Faculty of Science, University of Zurich, CH-8057, Switzerland

[6]Equal contribution

*Corresponding author

Vikram Govind Panse (vpanse@imm.uzh.ch)

Summary

Eukaryotic ribosome precursors acquire translation competence in the cytoplasm through stepwise release of bound assembly factors, and proofreading of their functional centers. In case of the pre-60S, these steps include removal of placeholders Rlp24, Arx1 and Mrt4 that prevent premature loading of the ribosomal protein eL24, the protein-folding machinery at the polypeptide exit tunnel (PET), and the ribosomal stalk, respectively. Here, we reveal that sequential ATPase and GTPase activities license release factors Rei1 and Yvh1 to trigger Arx1 and Mrt4 removal. Drg1-ATPase activity removes Rlp24 from the GTPase Nog1 on the pre-60S; consequently, the C-terminal tail of Nog1 is extracted from the PET. These events enable Rei1 to probe PET integrity, and catalyze Arx1 release. Concomitantly, Nog1 eviction from the pre-60S permits peptidyl transferase center maturation, and Yvh1 to mediate Mrt4 release for stalk assembly. Thus, Nog1 co-ordinates assembly, maturation and quality control of distant functional centers during ribosome formation.

Introduction

Error-free translation of the genetic code by the ribosome is critical for proteome homeostasis and cellular function. This essential task necessitates that only correctly assembled ribosomal subunits are committed for translation. Eukaryotic ribosome assembly is initiated by RNA-polymerase I driven production of pre-rRNA in the nucleolus (Pena et al., 2017, Kressler et al., 2017). The emerging pre-rRNA associates with small subunit (40S) specific r-proteins, snoRNAs, U3snoRNP, numerous U3 proteins (UTPs) and assembly factors to form a pre-40S. Endonucleolytic cleavage releases the earliest pre-40S, permitting the remaining growing pre-rRNA to recruit large subunit (60S) specific r-proteins and assembly factors to form a pre-60S. On their way through the nucleoplasm, pre-ribosomal particles interact with >200 assembly factors including >40 energy-consuming AAA-ATPases, ABC-ATPases, GTPases and ATP-dependent RNA helicases. Elucidating their order of action, and mechanisms that co-ordinate their activities during pre-ribosome maturation is an important challenge.

Export-competent pre-ribosomes are transported through nuclear pore complexes (NPCs) into the cytoplasm where they undergo maturation and proofreading before acquiring translation competence (Nerurkar et al., 2015). These steps include release of assembly factors, transport receptors, pre-rRNA processing steps and incorporation of remaining r-proteins critical for ribosome function. Cytoplasmic maturation of an exported pre-60S is initiated by the AAA-ATPase Drg1, which directly binds to and evicts the placeholder ribosomal-like protein Rlp24 from the pre-60S (Pertschy et al., 2007, Kappel et al., 2012, Kressler et al., 2012). This step is a prerequisite for the release of two GTPases Nog1 and Nug1, the assembly factor Nsa2, the subunit anti-association factor Tif6, the ribosomal-like protein Mrt4 and export factors Mex67-Mtr2, Bud20, Arx1 and Nmd3 (Loibl et al., 2014, Zisser et al., 2018). Following Rlp24 release, the 60S maturation pathway, *via* a yet unknown mechanism, bifurcates to proofread the polypeptide exit tunnel (PET) and assemble the ribosomal stalk (Lo et al., 2010). PET maturation is accomplished through the release of Arx1, an assembly factor that covers the tunnel, and prevents premature loading of the protein-folding chaperone machinery (Bradatsch et al., 2012, Greber et al., 2012).

Arx1 release from the pre-60S requires the cytoplasmic zinc-finger protein Rei1, the DnaJ domain-containing protein Jjj1 and Ssa1/Ssa2 (Hsp70) ATPase activity (Meyer et al., 2007, Meyer et al., 2010). Cryo-electron microscopy (cryo-EM) studies have revealed that Rei1 inserts its C-terminal tail (Rei1-CTT) into the PET (Greber et al., 2016). Failure to insert the Rei1-CTT into the tunnel impairs Arx1 release, and blocks subsequent pre-60S maturation (Greber et al., 2016). Cryo-EM analyses of a nuclear pre-60S revealed that the C-terminal tail of the GTPase Nog1 (Nog1-CTT) intertwines around Rlp24, makes contact with Arx1 and inserts its end into the PET (Wu et al., 2016). For Rei1-CTT to gain access to the PET, the Nog1-CTT end must be extracted. How these events are orchestrated during cytoplasmic maturation is unknown.

Another functional center whose assembly is completed in the cytoplasm is the 60S ribosomal stalk. The stalk is built from a single copy of ribosomal proteins uL10 (Rpp0) and two heterodimers of P1 (Rpp1) and P2 (Rpp2), and plays an essential role by recruiting and activating translation elongation factors. On a mature 60S subunit, the stalk is anchored through the interaction of uL10 with rRNA and uL11 (Rpl12) (Ben-Shem et al., 2011). During nuclear 60S assembly, the ribosomal-like protein Mrt4 functions as a placeholder for uL10 (Lo et al., 2009, Kemmler et al., 2009). Mrt4 removal from the pre-60S is triggered by the release factor Yvh1 (Kemmler et al., 2009); (Lo et al., 2009). Only after Mrt4 is released, uL10 can be loaded onto the pre-60S, to assemble the stalk. How stalk assembly is co-oordinated with other cytoplasmic maturation steps remains unclear.

Removal of placeholders Rlp24, Arx1 and Mrt4 from the pre-60S is an essential pre-requiste for PET maturation and quality control, polypeptidyl transferase centre (PTC) maturation, stalk assembly and incorporation of remaining r-proteins. How these spatially distant events on the pre-60S are orchestrated remains unknown. By employing quantitative mass spectrometry, genetic and cell-biological approaches, we reveal that the ATPase Drg1 and the GTPase Nog1 license these events, and ensure that only correctly assembled 60S subunits enter translation.

Results

The nuclear localized GTPase Nog1 co-enriches with a late pre-60S that contains export factors Nmd3, Bud20, Mex67-Mtr2 and Arx1 (Jensen et al., 2003, Kallstrom et al., 2003). In wild-type (WT) cells, Nog1 is not detected on a cytoplasmic pre-60S purified through tandem-affinity purification (TAP) of Lsg1 (Kressler et al., 2008, Altvater et al., 2012). However, it mis-localizes to the cytoplasm, and accumulates on Lsg1-TAP particles upon impairment of the cytoplasmic AAA-ATPase Drg1 or upon treating yeast cells with the Drg1-inhibitor diazaborine (DIA) (Pertschy et al., 2007, Loibl et al., 2014). These data show that Nog1 travels to the cytoplasm, where it is released in a Drg1-dependent manner and rapidly recycled back to the nucleus. How and exactly when Nog1 is released from the pre-60S in the cytoplasm is unclear.

Nog1^{DN} accumulates on a cytoplasmic pre-60S particle

The Nog1 G-domain exhibits characteristic G1-G5 motifs (Figure 1A, upper panel) suggesting that like other GTPases such as Nug2/Nog2 and Lsg1, GTP-binding or hydrolysis might regulate interactions between Nog1 and the pre-60S particle (Hedges et al., 2005, Matsuo et al., 2014). Dominant-negative mutations have been described within the G1 motif of Lsg1(K349N/R/T) (Hedges et al., 2005) and in the G3 motif of Nug2 (G369A) (Bourne et al., 1991, Hedges et al., 2005, Matsuo et al., 2014) that impair the release of these GTPases from a pre-60S. A G224A mutation in the G3 motif of human Nog1, which presumably blocks GTP hydrolysis, was shown to be dominant negative in mammalian cells, and induced pre-rRNA processing and assembly defects (Lapik et al., 2007).

We investigated whether the G-domain contributes to Nog1 release from the pre-60S in the cytoplasm. To this end, the orthologous mutation in the G3 motif (G223A) of yeast Nog1 (Figure 1A), hereafter termed Nog1^{DN}, was transformed into a Nog1 shuffle strain, wherein the *NOG1* gene was disrupted, but viability of the yeast cells maintained through a centromeric plasmid containing a WT copy of *NOG1*. We did not obtain transformants for the Nog1^{DN} mutant. To demonstrate dominant negative behavior, we placed the Nog1^{DN} mutant under the control of an inducible *GAL1* promoter, and transformed this plasmid into WT yeast cells. On glucose-containing medium,

where Nog1^{DN} expression is repressed, the resulting transformants grew similar to WT. In contrast, expression of Nog1^{DN} in galactose-containing medium was lethal to yeast cells (Figure 1B), confirming the dominant negative behavior of the G223A mutation.

Nog1 is recruited to the pre-60S in the nucleolus (Kressler et al., 2008, Altvater et al., 2012), and is released from the particle in the cytoplasm (Pertschy et al., 2007, Lo et al., 2010, Altvater et al., 2012). We investigated whether the Nog1^{DN} mutant was released from the pre-60S in the cytoplasm. For this, we isolated the Lsg1-TAP particle after inducing expression of either Nog1 or the Nog1^{DN} mutant allele for 2.5 hours (Figure 1C). Western analyses revealed that Nog1^{DN} mutant protein, but not Nog1 accumulated on the Lsg1-TAP particle (Figure 1C). Whole cell extracts (WCE) revealed similar Nog1 and Nog1^{DN} protein levels (Figure 1C), suggesting Nog1^{DN} co-enrichment with Lsg1-TAP is not due to altered expression of the mutant protein. Moreover, the Nog1^{DN}-GFP fusion showed an increase in cytoplasmic signal supporting the notion that Nog1^{DN} release from the pre-60S in the cytoplasm is impaired (Figure 1D). Although a nuclear signal of Nog1^{DN}-GFP is observed in these cells, this mutant did not efficiently co-enrich with Ssf1-TAP under the same conditions (Figure 1C), possibly due to blockage of downstream cytoplasmic maturation steps that indirectly impair early assembly steps (see later). We conclude that a functional G-domain is essential to evict Nog1 from the pre-60S in the cytoplasm.

Nog1^{DN} impairs cytoplasmic maturation of the pre-60S particle

We investigated consequences of impaired Nog1^{DN} release on the composition of the cytoplasmic Lsg1-TAP particle by Sequential Window Acquisition of all THeoretical fragment ion spectra mass spectrometry, also termed SWATH-MS. SWATH-MS is a mass spectrometry approach that combines data-independent acquisition with a peptide-centric data query strategy (Gillet et al., 2012). In contrast to selected reaction monitoring mass spectrometry (SRM-MS) (Picotti and Aebersold, 2012), SWATH-MS can be extended to the analysis of any peptide and protein of interest post-acquisition, while maintaining optimal consistency of quantification in pull-down samples (Collins et al., 2013, Lambert et al., 2013).

We interrogated quantitatively the protein composition of four well-characterized pre-60S particles representing different maturation stages (Nissan et al., 2002): Ssf1-TAP, an early nucleolar particle; Rix1-TAP, a nucleoplasmic particle; Arx1-TAP, a particle loaded with nuclear export factors and Lsg1-TAP, an exclusively cytoplasmic pre-60S. The data was analyzed using OpenSWATH software (Rost et al., 2014), and accuracy was compared with SRM-MS based analyses (Altvater et al., 2012). We found that the proteomic heat map obtained *via* SWATH-MS was in agreement with SRM-MS (Altvater et al., 2012) and Western analyses (Figure 2 - figure supplement 1). In contrast to SRM-MS, SWATH-MS permitted the quantitation of the approximate residence time of nearly all assembly factors along the 60S maturation pathway (Figure 2).

Next, we correlated the protein heat map with reported pre-ribosome cryo-EM structures (Sanghai et al., 2018, Kater et al., 2017, Wu et al., 2016, Barrio-Garcia et al., 2016, Ma et al., 2017, Malyutin et al., 2017, Greber et al., 2016). These analyses allowed organization of assembly factors into different clusters on a maturing pre-60S. For example, the early nucleolar Ssf1-Rrp14-Rrp15-Mak11 cluster, the nuclear ITS2 factors Nop15-Rlp7-Cic1-Nop7, the 5S RNP-associated Rrs1-Rpf2, the Rix1-Rea1 machinery and the Drg1-dependent factors Rlp24-Nog1-Nsa2-Bud20 appear to undergo coordinated and grouped release. Our analyses also revealed temporal association of assembly factors for which structural information in the context of the pre-60S is lacking. These factors include nucleolar proteins, and the uncharacterized nuclear localized Tma16 (Figure 2). We conclude that SWATH-MS is a reliable tool to quantify the protein contents of pre-ribosomal particles.

Next, we quantified and compared protein contents of genetically trapped cytoplasmic pre-60S particles isolated from yeast cells expressing either the dominant negative Drg1-E617Q, (Lsg1-TAP:Drg1^{DN}) (Altvater et al., 2012) or Nog1^{DN} (Lsg1-TAP:Nog1^{DN}) mutant. We focused on those assembly factors known to participate in pre-60S cytoplasmic maturation (Figure 3A). In agreement with previous studies (Pertschy et al., 2007, Lo et al., 2010, Altvater et al., 2012), a Drg1^{DN}:Lsg1-TAP particle accumulated Rlp24, Bud20, Nog1, Mrt4, Nmd3 and Tif6 (Figure 3A and Figure 3B). In addition, the cytoplasmic chaperone Sqt1 that loads uL16 onto the pre-60S (Pausch et al.,

2015), and the uncharacterized ribosome associated factor Tma16 (Fleischer et al., 2006) accumulated on the Drg1^{DN}:Lsg1-TAP particle (Figure 3B). Like the Drg1^{DN}:Lsg1-TAP particle, the Lsg1-TAP:Nog1^{DN} particle accumulated Mrt4, Sqt1, Tma16, Nmd3 and Tif6 (Figure 3A and Figure 3B). However, unlike the Drg1^{DN}:Lsg1-TAP particle, Rlp24 and its interaction partner Bud20 did not accumulate on the the Lsg1-TAP:Nog1^{DN} particle (Figure 3A and Figure 3B). Both Drg1^{DN} and Nog1^{DN}-trapped Lsg1-TAP particles failed to recruit Yvh1. While Rei1 recruitment to the Lsg1-TAP:Drg1^{DN} particle was impaired, Nog1^{DN}-trapped particles recruited Rei1 (Figure 3C). In contrast, Reh1, which functionally overlaps with Rei1 (Parnell and Bass, 2009) (Greber et al., 2016), accumulated on both Drg1^{DN} and Nog1^{DN}-trapped Lsg1-TAP particles (Figure 3B). The relative co-enrichments of assembly factors on the Lsg1-TAP:Nog1^{DN} particle monitored *via* SWATH-MS were in agreement with Western analyses (Figure 3C). These data suggest that Nog1^{DN} expressing cells are impaired in a subset of events along the 60S cytoplasmic maturation pathway.

Nog1^{DN} does not hinder initiation of cytoplasmic maturation

Cryo-EM studies have revealed that different domains of the assembly factor Nog1 (NTD, G-domain and CTT) meander from the peptidyl transferase centre (PTC) to the PET, and contact assembly factors on the pre-60S (Wu et al., 2016). The Nog1-NTD interacts with the assembly factor Nsa2, the Nog1-G domain contacts the ribosomal-like protein Mrt4, and the Nog1-CTT intertwines around Rlp24 and contacts Arx1 (Figure 1A). Although Nog1, Nsa2, Arx1, Bud20, Mrt4 and Rlp24 are recruited to the pre-60S already during nucleolar/nucleoplasmic maturation, this cluster of assembly factors (Figure 1A) is evicted only in the cytoplasm (Figure 3A) (Pertschy et al., 2007, Lo et al., 2010, Altvater et al., 2012).

To dissect the impact of impaired Nog1^{DN} release from the pre-60S on the cytoplasmic maturation pathway, we employed a cell-biological approach. Release of the ribosomal like-protein Rlp24 from the pre-60S initiates the cytoplasmic maturation cascade (Figure 3A) (Pertschy et al., 2007, Lo et al., 2010). On the pre-60S, Rlp24 directly contacts Bud20, and then intertwines around the Nog1-CTT forming a Nog1-CTT:Rlp24 complex (Figure 4A). The

last 40 residues of the Rlp24 C-terminal tail (155-190) that remain unresolved in cryo-EM structures (Wu et al., 2016, Zhou et al., 2019), recruit and activate the AAA-ATPase Drg1 to extract Rlp24 from the pre-60S (Pertschy et al., 2007, Lo et al., 2010, Kappel et al., 2012, Altvater et al., 2012). Given the intimate interactions between Nog1-CTT and Rlp24 on the pre-60S (Wu et al., 2016) (Figure 4A), we wondered whether Nog1^{DN} hinders Drg1-mediated Rlp24 release. As judged by immunofluorescence, Rlp24-TAP did not mis-localize to the cytoplasm upon Nog1^{DN} expression (Figure 4B) suggesting that Nog1^{DN} accumulation on a cytoplasmic pre-60S did not interfere with the release and recycling of Rlp24 back to the nucleus. These data are consistent with SWATH-MS analyses which show that Rlp24 does not accumulate on the Lsg1-TAP:Nog1^{DN} particle (Figure 3B). This finding is in agreement with previous studies which showed that Drg1-ATPase activity is necessary and sufficient to release Rlp24 from the pre-60S (Kappel et al., 2012). The presence of Nog1^{DN} on the pre-60S did not interfere with recruitment of r-protein eL24 (yeast Rpl24) as judged by Western analyses (Figure 3C). Cell-biological studies indicate that the release of the Rlp24-interacting assembly factor Bud20 from the pre-60S is also not impaired in Nog1^{DN} expressing cells (Figure 4C). We conclude that Nog1^{DN} does not disturb initiation of the pre-60S cytoplasmic maturation cascade.

While the Lsg1-TAP:Drg1^{DN} particle accumulated Rlp24, Drg1^{DN}, Nog1 and another GTPase Nug1 (Altvater et al., 2012), the Lsg1-TAP:Nog1^{DN} particle accumulated only Nog1^{DN,}, but not Rlp24, Drg1 and Nug1 (Figure 3B and Figure 4C). Based on these data, we conclude that Nog1^{DN} eviction from the pre-60S occurs after Drg1-mediated Rlp24 release.

Nog1^{DN} interferes with ribosomal stalk assembly

Following Drg1-mediated Rlp24 release from the pre-60S, cytoplasmic maturation pathway bifurcates to: (1) assemble the ribosomal stalk, and (2) mature and proofread PET integrity (Figure 3A); (Lo et al., 2010). The ribosomal stalk is assembled in the cytoplasm from the acidic r-proteins uL10 (yeast P0) and P1/P2 heterodimers. Mrt4 functions as a nuclear placeholder for uL10 and joins the pre-60S already in the nucleolus (Lo et al., 2010, Kemmler et al., 2009). Mrt4 release in the cytoplasm requires Yvh1, an

assembly factor that maximally co-enriches with Lsg1-TAP (Kemmler et al., 2009, Lo et al., 2010). SWATH-MS and Western analyses revealed that Lsg1-TAP:Nog1^{DN} failed to recruit Yvh1, and accumulated Mrt4 (Figure 3B and Figure 3C). In agreement with these data, we found that Nog1^{DN} expressing cells mislocalized Mrt4-GFP into the cytoplasm (Figure 4C). Accordingly, Western analyses showed that uL10 recruitment to Lsg1-TAP:Nog1^{DN} was impaired (Figure 3C). Cryo-EM studies suggest that Yvh1-binding site on the pre-60S clashes with the Nog1-G domain (Figure 4D) (Zhou et al., 2019, Kargas et al., 2019), providing an explanation as to why Nog1 eviction is critical for stalk assembly. Given that Drg1-ATPase activity is required to evict Nog1, these structural data explain why Drg1^{DN} expressing cells are impaired in Mrt4 release, and consequently stalk assembly (Altvater et al., 2012, Lo et al., 2010). We conclude that stalk assembly requires Drg1-ATPase activity and a functional Nog1-GTPase domain.

Nog1^{DN} does not impair PET maturation

We investigated the impact of Nog1^{DN} expression on PET maturation and quality control (Figure 3A). During nuclear assembly of the pre-60S, the aminopeptidase fold of Arx1 covers the PET (Bradatsch et al., 2012, Greber et al., 2012). Arx1 eviction from the pre-60S is triggered in the cytoplasm by Rei1 (Meyer et al., 2010). Rei1 is recruited to the pre-60S through its N-terminal domain (Lebreton et al., 2006), whereas its C-terminal tail-end (Rei-CTT) is inserted into the PET (Greber et al., 2016). Rei1 recruitment to the pre-60S requires Drg1-mediated Rlp24 release (Figure 5A) (Lo et al., 2010, Altvater et al., 2012). We found that Nog1^{DN} expression did not interfere with Rei1 recruitment (Figure 3B and Figure 3C). However, co-expression of Nog1^{DN} and Drg1^{DN} impaired Rei1 recruitment to the pre-60S (Figure 5A). Accordingly, Nog1^{DN} expressing cells when treated with the Drg1-inhibitor diazaborine (DIA) mis-localized Arx1-GFP to the cytoplasm in these cells (Figure 5B). Cryo-EM studies indicate that the Rei1 binding site on the pre-60S clashes with the Nog1-CTT:Rlp24 complex (Figure 5C) (Zhou et al., 2019), providing an explanation as to why PET maturation is inhibited in Drg1^{DN} (or DIA treated) expressing cells. All these data show that Rlp24

extraction from the Nog1-CTT is critical to recruit Rei1 to the pre-60S in order to initiate PET maturation.

Nog1^{DN} expressing cells did not mislocalize Arx1-GFP into the cytoplasm (Figure 5D) suggesting that Nog1^{DN} presence on the pre-60S does not interfere with the ability of Rei1-CTT to probe the PET. Failure to insert Rei1-CTT into the PET by attaching a bulky domain (*rei1-TAP*) blocks Arx1 release and progression of cytoplasmic maturation, suggesting that PET proofreading represents a quality control check point (Greber et al., 2016). Consistent with this, Nog1^{DN} expression in a *rei1-TAP* mutant (where Rei1-CTT function to probe the PET is compromised), mislocalized Arx1-GFP to the cytoplasm (Figure 5D). Before Rei1-CTT can probe PET integrity, the terminal end of Nog1-CTT needs to be extracted from the PET. Given that Rei1 recrutiment and PET probing is not impaired in Nog1^{DN} expressing cells we suggest that Nog1^{DN}-CTT has been removed from the PET, and this does not require a functional Nog1-G3 domain. We conclude that presence of Nog1^{DN} on the pre-60S does not hinder Rei1 recruitment, and insertion of the Rei1-CTT into the PET.

The Nog1-CTT:Rlp24 complex negatively regulates PET maturation

Nog1-CTT intertwines around the helical segements of Rlp24, then contacts Arx1 and finally inserts its terminal end into the PET (Figure 1A). We investigated which regions of Nog1-CTT contribute to pre-60S cytoplasmic maturation (Figure 6A and Figure 6B). We found that a Nog1 mutant lacking the entire CTT including the Rlp24 interacting region, Nog1$^{1-426}$, was lethal in yeast (Figure 6B). Over-expression of a Nog1 mutant lacking the Rlp24 interacting region, Nog1$^{\Delta 427-536}$, severely impaired growth of yeast in a dominant negative manner (Figure 6C). However, unlike the Nog1^{DN} mutant, Nog1$^{\Delta 427-536}$ expressing cells did not mislocalize Mrt4-GFP and Tif6-GFP to the cytoplasm (Figure 6C). Likewise, a Rlp24 mutant lacking Nog1-interacting helices, Rlp24$^{\Delta 91-105}$, also impaired yeast growth in a dominant negative manner (Figure 6A and Figure 6C). Expression of the Rlp24$^{1-146}$ mutant (Figure 6A) that lacks the Drg1-binding platform, and therefore cannot be extracted from pre-60S, mislocalized Arx1-GFP, Mrt4-GFP and Tif6-GFP to the cytoplasm (Figure 6C) (Lo et al., 2010). However, Rlp24$^{\Delta 91-105}$ expressing

cells did not mislocalize these factors to the cytoplasm (Figure 6C). Given that Nog1 and Rlp24 rely on each other for their recruitment to the pre-60S (Saveanu et al., 2003), the toxicity of Nog1$^{\Delta 427\text{-}536}$ and Rlp24$^{\Delta 91\text{-}105}$ mutants, very likely reflects a failure to form a Nog1-CTT:Rlp24 complex on the pre-60S during early nuclear maturation. In contrast to the lethal Nog1$^{1\text{-}426}$ mutant, yeast strains expressing Nog1-CTT truncation mutants containing the Rlp24 interacting region but lacking the rest of the CTT complemented the lethality of the *nog1*Δ strain, but induced impaired growth at 20ºC and 25ºC (Figure 6A and Figure 6B). In agreement with these observations, growth of the Nog1-GFP strain was severely impaired at these temperatures (Figure 6B). We monitored PET maturation (Arx1-GFP), stalk assembly (Mrt4-GFP) and Tif6-GFP localization after treating the Nog1$^{1\text{-}479}$ truncation mutant that retains the Rlp24 interaction platform, with DIA which impairs Drg1-mediated Rlp24 release. We found that Arx1-GFP mislocalised to the cytoplasm in these cells (Figure 6D) emphasizing the importance of Rlp24 release, and disassembly of the Nog1-CTT:Rlp24 complex for PET maturation. As expected, Mrt4-GFP and Tif6-GFP also mislocalised to the cytoplasm (Figure 6D), consistent with the idea that Nog1 release from the pre-60S requires Rlp24 removal. In conjunction with cryo-EM studies (Figure 5C), these data support the idea that Nog1-CTT:Rlp24 complex negatively regulates PET maturation.

Nog1^{DN} blocks the terminal cytoplasmic maturation steps

The terminal steps during cytoplasmic maturation of a pre-60S involve sequential release of the nuclear export signal (NES) containing Crm1 adaptor Nmd3 and the 60S anti-association factor Tif6 (Weis et al., 2015, Ma et al., 2017, Kargas et al., 2019). Nog1^{DN} expression accumulated Nmd3 and Tif6 on the pre-60S as judged by SWATH-MS and Western analyses (Figure 3B and Figure 3C). To monitor Nmd3 accumulation on a cytoplasmic pre-60S by cell-biological means, we employed the nuclear localized Nmd3^{3A}-GFP mutant fusion, which harbors mutations in its NES that decrease its nuclear export rate (Hedges et al., 2005). As expected, at steady state, Nmd3^{3A}-GFP and Tif6-GFP localize to the nucleus in cells expressing WT Nog1 (Figure 4C). However, in Nog1^{DN} expressing cells, Nmd3^{3A}-GFP and Tif6-GFP

mislocalised to the cytoplasm (Figure 4C). We suggest that the presence of Nog1^{DN} on the pre-60S impairs Nmd3 and Tif6 release.

Like Nog1^{DN} expressing cells, *yvh1Δ* cells mislocalize both Mrt4-GFP and Tif6-GFP to the cytoplasm, impairing stalk assembly and progression of the cytoplasmic maturation pathway (Kemmler et al., 2009, Lo et al., 2010). Given that Yvh1 recruitment to the pre-60S is impaired in Nog1^{DN} expressing cells, we investigated whether the dominant negative behavior of Nog1^{DN} is due to the failure to release Mrt4. To test this, we employed a dominant gain-of-function allele *MRT4^{G68E}* that bypasses Yvh1-mediated Mrt4 release from the pre-60S (Figure 7A and Figure 7B) and relocalizes Tif6-GFP to the nucleus (Figure 7A) (Kemmler et al., 2009). We found that Nog1^{DN} expression is toxic in *yvh1*ΔMRT4^{G68E} cells (Figure 7B). While Mrt4^{G68E}-GFP relocalised to the nucleus, Tif6-GFP still mislocalised to the cytoplasm in these cells (Figure 7A), showing that the presence of Mrt4 on the pre-60S is not the cause for the dominant negative behavior of Nog1^{DN}. Consistent with the sequential release of Nmd3 and Tif6 from the pre-60S, Western analyses show that Nmd3 accumulates on the Lsg1-TAP particle isolated from *yvh1*ΔMRT4^{G68E} cells expressing Nog1^{DN} (Figure 7C). Notably, the r-protein uL10 is recruited to this Lsg1-TAP particle (Figure 7C), indicating that Nog1^{DN} does not interfere with stalk assembly in *yvh1*ΔMRT4^{G68E} cells. In light of a recent cryo-EM study these data suggest that Nog1^{DN} presence on the pre-60S prevents rearrangement of rRNA helix H89, and sterically hinders incorporation of uL16 into its RNA-binding site (Figure 7D), a critical step that triggers downstream events that drive a pre-60S toward translation competence (Kargas et al., 2019, Zhou et al., 2019).

Discussion

During its journey from the nucleolus to the cytoplasm and concomitant progression towards the mature subunit, a pre-60S interacts with diverse energy-consuming enzymes. However, the precise order of recruitment and eviction, as well as mechanisms that co-ordinate different energy-consuming steps remain unknown. Here, we reveal that sequential Drg1-ATPase and Nog1-GTPase acitivities license early cytoplasmic maturation events that eventually drive a pre-60S towards translation competence.

Nog1 eviction requires a functional G-domain and Drg1-ATPase acitivity

The GTPase Nog1 travels into the cytoplasm with the pre-60S where it is released in a Drg1-ATPase manner and recycled back into the nucleus(Pertschy et al., 2007, Lo et al., 2010). Our finding that the dominant negative Nog1^{DN} (Nog1G223A) mutant accumulates on Lsg1-TAP (Figure 1C) supports the notion that an impaired G-domain does not hinder recruitment to the assembling pre-60S particle. Instead, like other GTPases involved in the 60S maturation pathway (Hedges et al., 2005, Matsuo et al., 2014), an impaired G3 domain blocks Nog1 release from the pre-60S. We and others (Lapik et al., 2007) have been unable to detect GTPase activity of recombinant Nog1 *in vitro*. Similar to its bacterial homologue ObgE, it could be that GTP hydrolysis is triggered only in context of the pre-ribosome (Feng et al., 2014). Nog1 is a predicted potassium-selective cation-dependent GTPase (also referred to as Group I CD-GTPase) (Ash et al., 2012). Group I CD-GTPases can be identified by the presence of two conserved asparagine residues in the G1 motif (Ash et al., 2012). The first of the two conserved asparagine residues (Asn^{K}) is coordinated to the potassium ion, whereas the second asparagine (Asn^{SwI}) facilitates the Switch I structure. In yeast Nog1, Asn^{K} is present (N177), however, the asparagine Asn^{SwI} is substituted with an arginine (R185). This raises the possibility that the second asparagine (or equivalent) might be provided by a yet unknown activator. The equivalent G223A mutation in the G3 motif reported here is also dominant negative in the Ras GTPase (Ford et al., 2005). Structural studies of this mutant revealed that the switch region adopts an open conformation preventing GTP from inducing an active confirmation (Ford et al., 2005) that sequesters Ras GEFs into non-productive complexes leading to the depletion of their intracellular pool (Ford et al., 2005). It would be interesting to determine the molecular basis that underlies Nog1^{DN} dominant negative nature, and if it is similar to the Ras^{G60A} mutant.

Nog1, whose GTPase domain is docked at the P0 stalk base at a similar position as bacterial ObgE, is remarkably unique with its CTT, which wraps around half the 60S subunit, passing by the PTC and entering the PET

(Wu et al., 2016) (Figure 1A). Covering a total distance of >250 Å, the CTT contacts Rlp24, Bud20, Tif6 and Arx1 (Figure 1A). Nog1-CTT intertwines with the C-terminal helices of Rlp24 forming a Nog1-CTT:Rlp24 complex on the pre-60S (Figure 4A). Intriguingly, despite these intimate interactions, we found that Rlp24 and Nog1^{DN} are independently released from the pre-60S. Previous work showed that Drg1 grips Rlp24 *via* its C-terminus, and then triggers its ATP-dependent release from the pre-60S (Kappel et al., 2012). Drg1^{DN} expression prevents the release of both Rlp24 and Nog1 from the pre-60S, suggesting that Nog1 eviction also requires Drg1-ATPase activity (Pertschy et al., 2007, Altvater et al., 2012). A recent cryo-EM study identified an early cytoplasmic pre-60S state in which Nog1-CTT was inserted into the PET, but the Nog1-NTD and Nog1-G domains were displaced from the pre-60S (Zhou et al., 2019). However, in this particle, Nog1-CTT intertwines around Rlp24, providing an explanation as to why Nog1 remains bound to the pre-60S. We suggest that Nog1 eviction from the pre-60S requires a functional Nog1 G-domain and Drg1-mediated extraction of Rlp24.

Another factor that makes contacts with Rlp24 is the export factor Bud20 (Altvater et al., 2012, Bassler et al., 2012). It seems likely that Bud20 release from the pre-60S is a consequence of Rlp24 release. Consistent with this, Drg1^{DN} expression interferes with both Rlp24 and Bud20 release and recycling from the pre-60S. Given that localization of Rlp24 and Bud20 is not altered upon Nog1^{DN} expression (Figure 4C), we suggest that Bud20 release from the pre-60S occurs prior to bifurcation of the cytoplasmic maturation pathway.

The Nog1-CTT:Rlp24 complex gates PET quality control

Drg1^{DN} expression impairs Rei1 recruitment to the pre-60S and consequently Arx1 release (Altvater et al., 2012). Drg1-mediated Rlp24 extraction from the Nog1-CTT:Rlp24 complex permits Rei1 recruitment to the pre-60S, and subsequently the Rei1-CTT to probe PET integrity for Arx1 release. Rei1 recrutiment to the pre-60S is unaffected in Nog1^{DN} expressing cells. Given that PET maturation is successfully accomplished in Nog1^{DN} expressing cells, we suggest that Nog1^{DN}-CTT has been extracted from the PET as a consequence of Rlp24-extraction from the pre-60S. Thus, Nog1

eviction from the pre-60S is not required to accomplish PET maturation.

Recent cryo-EM studies revealed that the cytoplasmic localized assembly factor Reh1, which functionally overlaps with Rei1 (Parnell and Bass, 2009, Greber et al., 2016) also inserts its C-terminal tail into the PET (Ma et al., 2017, Kargas et al., 2019). Our SWATH-MS data indicate that Reh1 accumulates on the Lsg1-TAP:Nog1^{DN} particle (Figure 3B) supporting the notion that Reh1 release occurs after Nog1 release from the pre-60S. These data are consistent with the idea that the PET is under continuous surveillance through sequential interactions with Nog1-CTT, Rei1-CTT and Reh1-CTT.

Nog1 gates stalk assembly and PTC maturation

Stalk assembly requires prior release of Mrt4 that is facilitated by the release factor Yvh1 (Lo et al., 2009, Kemmler et al., 2009). Nog1^{DN} expression interferes with Yvh1 recruitment to the pre-60S particle, and therefore impairs Mrt4 release (Figure 4C and Figure 4D). Cryo-EM studies have revealed that the presence of Nog1 prevents the pre-60S from recruiting Yvh1, as both factors localize close to the stalk base and obstruct the Yvh1 binding site (Figure 4D) (Kargas et al., 2019, Zhou et al., 2019). Given that Nog1 release is impaired in Drg1^{DN} expressing cells (Altvater et al., 2012), these data provide an explanation as to why stalk assembly is impaired in these cells.

While, Mrt4^{G68E} efficiently bypassed the need for Yvh1-mediated release, this gain-of-function allele did not rescue the dominant negative phenotype of Nog1^{DN} (Figure 7B). These cells were still impaired in Nmd3 and Tif6 release from the pre-60S (Figure 7A and Figure 7C). Retention of Nog1^{DN} on the pre-60S prevents rearrangement of rRNA helix H89, and sterically hinders uL16 incorporation. Stable accommodation of uL16 into the pre-60S is a critical event to re-orient rRNA helices H89 and H38, that permits a conformational rearrangement of the Nmd3 C-terminal domain (Malyutin et al., 2017, Zhou et al., 2019, Kargas et al., 2019). This rearrangement triggers the GTPase Lsg1 to evict Nmd3, and subsequently license Efl1/Sdo1-to mediate Tif6 release. Notably, the dedicated chaperone Sqt1 that guides incorporation of uL16 into the pre-60S accumulates on the Lsg1-TAP:Nog1^{DN}

particle (Figure 3B). In light of these data and work from the Kressler laboratory (Pausch et al., 2015), it is tempting to speculate that a pre-formed Sqt1:uL16 complex docks on the pre-60S. Nog1 eviction permits transfer of uL16 into its RNA-binding site, and release of its dedicated chaperone Sqt1. We suggest that Nog1 release from a pre-60S licenses stalk assembly and downstream maturation steps critical to acquire translation competence.

SWATH-MS analyses allowed the identification of assembly factors whose release or recruitment appears to be dependent on the release of the GTPase Nog1 from cytoplasmic pre-60S particles. These include assembly factors Sqt1, Mex67, Ecm1, Tma16 and Arb1 for which structural information in context of a pre-60S is lacking. In contrast to Sqt1, Mex67, Ecm1 and Tma16 which accumulated on the Lsg1-TAP Nog1^{DN} particle, we found that recruitment of the ABC-ATPase Arb1 was impaired (Figure 3B). Arb1 has been implicated in both 40S and 60S subunit assembly (Dong et al., 2005). A recent cryo-EM structure of a translationally stalled-mature 60S subunit shows that Arb1 docks in a region of rRNA which overlaps with the binding site of Nmd3 on the pre-60S (Su et al., 2019). We speculate that Nog1 release, stable uL16 incorporation and Nmd3 release precede Arb1 recruitment to the pre-60S.

Nog1 co-ordinates assembly, maturation and quality control of distant ribosomal centres

Previously, the Johnson laboratory had ordered cytoplasmic maturation events on the pre-60S into a coherent pathway (Lo et al., 2010). In that pioneering study, AAA-ATPase Drg1 activity was proposed to initiate two parallel branches of the pathway i.e. PET maturation with quality control and ribosome stalk assembly (Figure 3A). The two branches converge to initiate Nmd3 and Tif6 release prior to acquiring translational competence. Our data suggest that Nog1 plays a pivotal role in coordinating bifurcation and convergence of the 60S cytoplasmic maturation pathway. Cryo-EM structures and the data presented here permit refinement of early events that drive the cytoplasmic pre-60S maturation (Figure 8). Upon arrival in the cytoplasm, the pre-60S recruits Drg1 via the C-terminal region of Rlp24. This interaction stimulates Drg1 ATPase activity resulting in Rlp24 removal, and as a

consequence the terminal end of Nog1-CTT is extracted from the PET (State I to State II). Removal of Rlp24 permits Rei1 recruitment, and Rei1-CTT to probe PET integrity to trigger Arx1 release through the the J-domain protein Jjj1 and ATPases Ssa1/2 (State III) (Meyer et al., 2007, Greber et al., 2016). Release of Rei1 then permits the assembly factor Reh1 to probe the PET (State IV) (Ma et al., 2017, Kargas et al., 2019). Nog1 eviction from the pre-60S requires extraction of Rlp24 from Nog1-CTT by the ATPase Drg1 and GTP hydrolysis within the Nog1-G domain. This event unleashes a sequence of events in different regions of the pre-60S: (1) it permits recruitment of the release factor Yvh1 to the pre-60S in order to mediate Mrt4 release, and initiate stalk assembly (State IV to State V), (2) it permits loading of r-proteins eL40 and uL16 into their rRNA binding sites (State V), (Zhou et al., 2019, Kargas et al., 2019), (3) it re-orientates rRNA helices H89 and H38 to promote a conformational rearrangement of the Nmd3 C-terminal domain (Malyutin et al., 2017, Zhou et al., 2019, Kargas et al., 2019) leading to Nmd3 eviction, thus completing PTC maturation (State V to State VI). We therefore propose that Nog1 serves as a hub that coordinates spatially distant maturation events to ensure only correctly assembled 60S subunit enter translation.

Finally, Nsa2 and Reh1 accumulate on Lsg1-TAP in $Drg1^{DN}$ as well as $Nog1^{DN}$ expressing cells (Altvater et al., 2012; Figure 3C). These data are consistent with the idea that Nog1 eviction from the pre-60S precedes Nsa2 and Reh1 release. However, the precise mechanisms that drive Nsa2 and Reh1 release remain unknown.

Nmd3 release licenses Efl1/Sdo1 to mediate Tif6 release (State VI) (Kargas et al., 2019). Although Lsg1 appears to be required for only during a specific step of the cytoplasmic maturation pathway, it seems that it can be recruited to a newly exported pre-60S. Lsg1 recruitment to the pre-60S does not seem to depend on the initial cytoplasmic maturation events such as Rlp24 extraction by Drg1, and Nog1 release, as we efficiently isolated $Drg1^{DN}$ and $Nog1^{DN}$ trapped particles via Lsg1-TAP (Altvater et al., 2012) (Figure 3B). These purifications suggest that the GTPases Nog1 and Lsg1 can bind simultaneously to cytoplasmic pre-60S particles.

Co-ordination between energy consuming enzymes ?

Strikingly, the release of the GTPase Nug2 from the pre-60S in the nucleus was reported to require its own GTPase activity, and the ATPase activity of the AAA-ATPase Rea1 (Matsuo et al., 2014). Nug2 binds the pre-60S at a site, which partially overlaps with the binding site for the NES containing adaptor Nmd3 (Sengupta et al., 2010). Only after Nug2 release, Nmd3 can be recruited to the pre-60S, a critical step that drives pre-60S nuclear export. In this case, coupled ATPase and GTPase activities, together with components of this assembly factor cluster (Figure 2), form a nuclear checkpoint to prevent a pre-60S, from prematurely acquiring export competence. Similar to Nug2, our data point to Nog1 release from the pre-60S presumably requiring its own GTPase activity, and the ATPase activity of the AAA-ATPase Drg1. Failure to release Nog1 blocks a specific branch of the cytoplasmic maturation pathway, and consequently PTC formation.

In contrast to their prokaryotic counterparts, eukaryotic ribosome formation requires the concerted efforts of >200 assembly factors and >40 ATPases, GTPases, ATP-dependent RNA helicases and kinases that interact with pre-ribosomes at distinct maturation steps. Our work flow of combining genetic trapping with SWATH-MS provides a powerful tool to uncover the intricate coordination between energy-consuming enzymes to sequentially release assembly factor clusters from maturing pre-ribosomes, and thereby reveal checkpoints during ribosome formation.

Material and Methods

Yeast strains and plasmids

The *Saccharomyces cerevisiae* strains used in this study are listed in Supplementary File 1. Genomic disruptions, C-terminal tagging and promoter switches at genomic loci were performed according to established protocols (Janke et al., 2004, Longtine et al., 1998, Puig et al., 2001).

Plasmids used in this study are listed in Supplementary File 2. Details of plasmid construction will be provided upon request. All recombinant DNA techniques were performed according to established procedures using *E. coli* XL1 blue cells for cloning and plasmid propagation. Mutations in *NOG1* and

RLP24 were generated using the QuikChange site-directed mutagenesis kit (Agilent Technologies, Santa Clara, CA, USA). All cloned DNA fragments and mutagenized plasmids were verified by sequencing.

Fluorescence microscopy

For assessing the localization of PGAL1-Nog1G223A-GFP, BY4741 cells were transformed with YEP351-Nog1-GFP and YEP351gal-Nog1G223A-GFP and grown in SR medium until OD600 = 0.4-0.6, induced for 30 min with 2% galactose. Cells were then washed once in YPD and incubated in YPD for 3 hours before imaging. For assessing localization of assembly factors, endogenously GFP-tagged strains were transformed with PGAL1 plasmids and were grown in SR medium until OD600=0.2-0.4 and then induced with 2% galactose for 3 hours. For $Nmd3^{3A}$-GFP visualization, a Nmd3 shuffle strain was transformed with $Nmd3^{3A}$ –GFP (NMD3I493A L497A L500A) and transformants were applied on FOA plates to shuffle out the wild-type *NMD3*. The resulting $Nmd3^{3A}$-GFP strain was transformed with PGAL1 plasmids and grown the same as the endogenously GFP-tagged strains. For experiments with Diazaborine, cells were incubated 1 hour prior to imaging with either DMSO or with 370 µM Diazaborine (dissolved in DMSO; M. Peter, ETH Zürich, Switzerland) in 1 ml of cell culture for 1 hour at 30°C on shaker. When cells were ready to be harvested, the pellet was washed one with H2O. 3 µl of cells were transferred on a microscopy slide (VWR) covered with a glass slip (18x18 mm no 1, VWR).

Rlp24-TAP localization was assayed by indirect immunofluorescence. The Rlp24-TAP strain was transformed with pGAL1-containing plasmids, and cultures were grown in the appropriate conditions to OD600 = 0.4-1. After adding formaldehyde (final conc. 4%) to the cultures, cells were fixed for 30 min at 30°C. Cells were then centrifuged, and incubated with 1ml of 0.1M KPi pH 6.4 with 3.7% Formaldehyde for 15 min at 30°C. Cells were then washed twice with 0.1M KPi pH 6.4 and once in spheroplasting buffer (0.1 M KPi pH7.4, 1.2 M Sorbitol, 0.5 mM MgCl2). The pellet was resuspended in 200 µl spheroplasting buffer and was either stored at -20°C or directly processed for spheroplasting. For spheroplasting, 2 µl of 1M DTT was added to the 200 µl

cells and incubated for 15 min at 30°C. Zymolyase 100T was added (final conc. 50 µg/ml) to the 200 µl and incubated for 10 min. Cells were quickly checked under the microscope to see whether spheroplasts were formed (spheroplasts appear black), otherwise incubated for a longer time, but no longer than 20 min. Then, the spherolplasts were centrifuged for 2 min 2000 rpm, washed and resuspended in spheroplasting buffer. 20 µl of poly-L-lysine (0.1% (w/v), Sigma-Aldrich) was applied per well on slides (8 well, 6 mm Menzel-Gläser Diagnostika, Brauschweig, Germany), incubated for 5 min, washed three times with dH2O, aspirated and air-dried. Approximately 40 µl of spheroplasts were added onto lysine-coated slide well. Non-adhering cell were removed after 30 seconds and the slide was incubated in an ice-cold methanol bath for 6 min before it was transferred to an ice-cold acetone bath for 10 seconds. The slide was air-dried and processed with 30 µl BSA/PBS (1x PBS, 1% w/v BSA) for 30 min in the dark at RT in a humid chamber. The blocking solution was removed, and primary antibody (anti-CBP 1:1000; Thermo Scientific, Rockford, IL, USA) in BSA/PBS was added to the wells and incubated for at least an hour (up to overnight) at RT in the dark. Wells were washed 3 times with BSA/PBS and incubated with secondary antibody AlexaFluor568 coupled anti-rabbit (Molecular Probes, Inc., Eugene, OR, US) at RT in the dark. After washing, cells were incubated for 30S with DAPI (1 µg/ml in BSA/PBS; Sigma-Aldrich). Wells were washed three times with BSA/PBS and dried before the slides were mounted with Mowiol (Calbiochem, San Diego, CA, USA).

Fluorescence signal was examined using a Leica DM6000B microscope fitted with a 63x 1.25 NA 1.30-0.60 NA oil immersion lens (HCX PL Fluotar; Leica). Pictures were acquired with a digital camera (ORCA-ER; Hamamatsu Photonics) and with Openlab software (Perkin Elmer) or with Leica LAS software. Representative sections were selected using ImageJ software and processed in AdobePhotoshop. Corresponding differential interference contrast (DIC) pictures were taken for each fluorescence image. All cell-biological studies were performed at least on three different occasions and in triplicates; >90% of cells showed the reported phenotypes in a sample size of >1000 cells. A summary of the quantification of all the cell-biological data is listed in Supplementary File 3.

690

691 **Biochemical analyses**

692 Whole cell extracts were prepared by alkaline lysis of yeast cells
693 (Kemmler et al., 2009). Tandem affinity purifications (TAP) of pre-ribosomal
694 particles were carried out as previously described (Faza et al., 2012, Altvater
695 et al., 2014). Calmodulin-eluates were separated on NuPAGE 4-12% Bis-Tris
696 gradient gels (Invitrogen, Carlsbad, CA, USA) and visualized by either Silver
697 staining or Western analyses using indicated antibodies. All biochemical
698 purifications were performed at least on three different occasions and in
699 triplicates. To analyze the samples by SWATH-MS proteins TEV eluates were
700 precipitated using trichloroacetic acid (TCA), washed once in cold acetone, air
701 dried and processed further (see paragraphs on SWATH-MS analyses).

702 Western analyses were performed as previously described (Kemmler
703 et al., 2009). The following antibodies were used: α-Mex67 (1:5,000; C
704 Dargemont, Institut Jacques Monod, Paris, France), α-Nmd3 (1:5,000; A
705 Johnson, University of Texas at Austin, Austin, TX, USA), α-Nog1 (1:1,000; M
706 Fromont-Racine, Institut Pasteur, Paris, France), α-Nop7 (1:2,000; B Stillman,
707 Cold Spring Harbor Laboratory, New York, NY, USA), α-Nug1 (1:1,000; this
708 study), France), α-Tif6 (1:2,000; GenWay Biotech, San Diego, CA, USA), α-
709 Yvh1 (1:4,000; Altvater et al., 2012), α-Rpl1 (1:10,000; F Lacroute, Centre de
710 Génétique Moléculaire du CNRS, Gif-sur-Yvette, France), α-Rpl3 (1:5,000; J
711 Warner, Albert Einstein College of Medicine, Bronx, NY, USA) and α-Rpl35
712 (uL29) (1:4,000; Altvater et al., 2012), α-Gsp1 (1:3,000; rabbit; Fischer et al.,
713 2015), α- Nsa2 (1:2000; M. Fromont-Racine, Institut Pasteur, Paris, France),
714 α-GFP (1:2000; Roche); α-FLAG (1:2000; Sigma). The secondary HRP-
715 conjugated α-rabbit and α-mouse antibodies (Sigma-Aldrich, St. Louis, MO,
716 USA) were used at 1:1,000-1:5,000 dilutions. Protein signals were visualized
717 using Immun-Star HRP chemiluminescence kit (Bio-Rad Laboratories,
718 Hercules, CA, USA) and captured by Fuji Super RX X-ray films (Fujifilm,
719 Tokyo, Japan) or using ImageQuant LAS 4000 (GE Healthcare).

720

721 **Sample preparation for the SWATH-MS analyses**

722 The proteins were solubilized in a denaturing buffer containing 8 M
723 urea and 0.1 M NH4HCO3. They were then reduced with 12 mM DTT at 37°C

for 30min and alkylated with 40 mM iodacetamide at room temperature in the dark for 30min. The samples were then diluted with 0.1 M NH4HCO3 to reach a final urea concentration of 1M and digested with sequencing grade porcine trypsin (Promega, 1:100 trypsin:protein). Digestion was stopped by adding formic acid to a final concentration of 1% (pH ~2). Peptides were desalted using macro spin columns (Nest group) according to the following procedure: Cartridges were wetted with one volume (350 µl) 100% methanol, washed with two volumes of 80% acetonitrile, 0.1% formic acid (FA) and equilibrated with three volumes of 0.1% FA. The acidified peptides were loaded twice on the cartridge, washed with three volumes 0.1% FA and eluted with two volumes 50% acetonitrile, 0.1% FA. Peptide were dried in a speedvac concentrator and resolubilized in 10 µl of 0.1% formic acid. The samples were then transferred to an MS vial and spiked with 1:20 (v:v) of iRT peptides (Escher et al., 2012).

Mass spectrometry data acquisition

1 µg of peptides were injected on a 5600 TripleTof mass spectrometer (ABSciex, Concord, Ontario) interfaced with an Eksigent NanoLC Ultra 1D Plus system (Eksigent, Dublin, CA). The peptides were separated on a 75-µm-diameter, 20 cm long New Objective emitter packed with Magic C18 AQ 3 µm resin (Michrom BioResources) and eluted at 300nl/min with a linear gradient of 5-to-35% Buffer A for 120min (Buffer A: 2% acetonitrile, 0.1% formic acid; Buffer B: 98% acetonitrile, 0.1% formic acid). MS data acquisition was performed in either data-dependent acquisition (DDA, top20, with 20 s dynamic exclusion) or data-independent acquisition (DIA) SWATH-MS mode (32 fixed precursor isolation windows of 25Da width (+1 Da overlap) each acquired for 100ms plus one MS1 scan acquired for 250ms) as described in (Gillet et al., 2012). The mass ranges recorded were 360-1460 m/z for MS1 and 50-2000 m/z for MS2. For either mode, the collision energy was set to 0.0625 × m/z - 6.5 with a 15-eV collision energy spread regardless of the precursor charge state.

SWATH-MS assay library generation

The DDA data recorded as described above were used to generate an assay library essentially as described (Schubert et al., 2015). In short, the raw DDA files were converted to mzXML using the qtofpeakpicker component of msconvert (ProteoWizard v 3.0.9987). The converted files searched with Comet (2014.02 rev. 0) and Mascot (version 2.5.1) using the yeast SGD database (release 13.01.2015) containing 6,713 proteins plus one protein entry for the concatenated sequence of the iRT peptides and as many decoy protein entries generated by pseudo-reversing the tryptic peptide sequences. The search parameters were as follows: +/- 25ppm tolerance for MS1 and MS2, fixed cysteine carbamidomethylation, variable methionine oxidation, semi-tryptic and up to 2 missed cleavages per peptide allowed. The Comet and Mascot search results were further processed using peptideProphet (Keller et al., 2002) and aggregated using iProphet (Shteynberg et al., 2011) (TPP v4.7 rev 0). The search results were filtered for an iProphet cutoff of 0.877603, corresponding to a 1% protein false discovery rate (FDR) estimated by MAYU (Reiter et al., 2009). The search results contained 22,961 peptides matching to a set of 2,610 proteins. The consensus spectral library was generated using SpectraST (Lam et al., 2008) and the assay library thereof was exported using the spectrast2tsv.py script (Schubert et al., 2015) with the following parameters: 6 highest intensity fragments (of charge 1+ or 2+) per peptide, within the mass range 350-2000 m/z and excluding the fragments within the precursor isolation window of the corresponding swath. The final library contains assays for 23,960 peptide precursors (thereof 21,472 proteotypic precursors covering 2,209 unique proteins). The assay library was exported to TraML format with shuffled decoys appended as described (Schubert et al., 2015).

SWATH-MS data analysis

The SWATH-MS data was extracted with the above-mentioned assay library through the iPortal interface with openSWATH (Rost et al., 2014) (openMS 2.1.0), pyProphet (Teleman et al., 2015) and TRIC alignment(Rost et al., 2016) using the same parameters as described in (Navarro et al., 2016). The SWATH identification results were further filtered to keep all the peptide assays with m-score below 0.01 for the protein entries with at least

one peptide with an m-score below 0.00000208508 (corresponding to a protein FDR of 1%). A set of ribosomal proteins (RPL28, RPL14B, RPL14A, RPL3, RPL19A/RPL19B, RPL35A/RPL35B, RPL12A/RPL12B, RPL27A/RPL27B, RPL2B/RPL2A, RPL14A/RPL14B, RPL7B/RPL7A, RPL1A/RPL1B) was used to normalize (mean-centering) the data as described in (Altvater et al., 2012). Only the proteotypic peptides were then kept, as well as the assays identified in the three triplicates for at least one AP-MS condition. Finally, proteins with less than 2 peptides were filtered out. The missing values for each peptide assay were imputed using a random value between 0.7 and 0.9 fold the lowest intensity of that peptide assay throughout the dataset. All the peptide assays values were then summed to a protein intensity value and a protein intensity mean per AP-MS condition. For the general protein heatmaps, each protein intensity was normalized to that of the highest protein value for the reported set. For the bar plots, the fold changes were calculated for each protein to that of the AP-MS condition with the highest protein intensity while the standard deviations were calculated per condition.

Data availability

All SWATH-MS data generated in this study have been deposited to the ProteomXchange Consortium via the PRIDE partner repository with the dataset identifier PXD011382.

Figure Legends

Figure 1. Nog1^{DN} accumulates on a cytoplasmic pre-60S. (A) Domain organization and location of Nog1 on a pre-60S (PDB-3JCT). NTD: N-terminal domain; CTT: C-terminal tail. The black arrow points to the G223A mutation in the G3 motif within the G-domain of Nog1. Selected assembly factors Mrt4, Nsa2, Tif6, Rlp24, Bud20, Arx1 bound to the pre-60S are shown in colour. **(B)** NOG1-G223A (NOG1^{DN}) is dominant negative. Wild-type cells were transformed with a plasmid encoding NOG1 or NOG1^{DN} under control of the galactose-inducible GAL1 promoter and spotted in 10-fold dilutions on glucose- or galactose-containing media. Plates were incubated at 30°C for 2-4

days. **(C)** Nog1^{DN} accumulates on a cytoplasmic pre-60S. Early nucleolar (Ssf1-TAP) and cytoplasmic (Lsg1-TAP) particles were isolated from either Nog1 or Nog1^{DN} expressing cells. Co-enrichment of Nog1 was investigated by Western blotting. Whole-cell extracts (WCEs) depict Nog1 protein levels in the indicated strains. **(D)** Nog1^{DN}-GFP accumulates in the cytoplasm. Wild-type cells expressing either Nog1-GFP or Nog1^{DN}-GFP under control of GAL1 were grown in raffinose-containing synthetic medium to early log phase and then supplemented with 2% galactose. After 30 min incubation, cells were washed, incubated in YPD for 3h and then visualized by fluorescence microscopy. Scale bar = 5 µm. Quantification is listed in Supplementary File 3. Whole-cell extracts (WCE) depict Nog1 protein levels in the indicated strains.

Figure 2. Association of assembly factors with pre-60S at different maturation stages revealed by SWATH-MS. Pre-60S particles representing nucleolar (Ssf1-TAP), nuclear (Rix1-TAP), nuclear to cytoplasmic (Arx1-TAP) and cytoplasmic (Lsg1-TAP) stages were analysed by SWATH-MS. A heat map was generated based on the average of three independent biological replicates and depicts the relative and individual enrichment of assembly factors with maturing pre-60S particles. The acquired SWATH data was normalized based on the average intensities of three depicted 60S r-proteins and the intensity of each factor was scaled to the highest intensity of that factor in the selected condition represented in the heat map. Maximum enrichment is depicted as purple and minimum enrichment as gold. Assembly factors with similar maximum enrichment profiles were then manually grouped into clusters based on available cryo-EM data (nucleolar pre-60S: PDB-6C0F and PDB-6ELZ; nuclear pre-60S: PDB-3JCT and PDB-5FL8; cytoplasmic pre-60S: PDB-5H4P, PDB-5T62, PDB-5APN, PDB-6RZZ and PDB-6N8N). ¥ depicts factors whose protein levels were analysed by Western blotting (Figure 2- figure supplement 1).

Figure 3. Nog1^{DN} impairs cytoplasmic maturation of a pre-60S. (A) Current model for the cytoplasmic maturation pathway of a pre-60S. A cytoplasmic pre-60S at different maturation stages is represented as a cartoon. Energy-consuming assembly factors are indicated with ATP or GTP.

Events that are impaired by Drg1^{DN} and Nog1^{DN} expression are highlighted in blue and red, respectively. **(B)** SWATH-MS analysis of Lsg1-TAP pre-60S in Drg1^{DN} and Nog1^{DN} expressing cells. Assembly factors accumulating on the pre-60S particle in a Drg1- or Nog1-dependent manner were clustered based on their increased enrichment. **(C)** Western analyses of selected pre-60S assembly factors involved in cytoplasmic maturation. Nog1^{DN}-trapped Lsg1-TAP particles were subjected to Western analysis using indicated antibodies. CBP: calmodulin binding peptide present in the Lsg1 TAP-tag.

Figure 4. Nog1^{DN} impairs stalk assembly and terminal maturation steps. **(A)** Cryo-EM structure (PDB-3JCT) of Nog1-containing pre-60S particle depicting the interaction between Rlp24 and Nog1. **(B)** A RLP24-TAP strain expressing NOG1 or NOG1^{DN} under control of GAL1 was grown in raffinose-containing synthetic medium to early log phase, then supplemented with 2% galactose, and further grown for 3h. Cells were then fixed and prepared for indirect immunofluorescence using an anti-Protein A antibody. Cells were visualized by fluorescence microscopy. Scale bar = 5 µm. Quantification is listed in Supplementary File 3. **(C)** Indicated GFP-tagged strains expressing NOG1 or NOG1^{DN} under control of GAL1 were grown as in (b) and then visualized by fluorescence microscopy. Scale bar = 5 µm. Quantification of the data is listed in Supplementary Table 2. **(D)** Yvh1 clashes with Nsa2:Nog1-G domain. Cryo-EM structures of nuclear Nog1-containing (PDB-3JCT) and late cytoplasmic Yvh1-containing (PDB-6RZZ) pre-60S particles were superimposed. Release of Nsa2:Nog1-G domain complex allows recruitment of Yvh1 to the pre-60S.

Figure 5. Nog1^{DN} does not impair PET maturation and quality control. (A) Drg1^{DN} impairs Yvh1 and Rei1 recruitment, whereas Nog1^{DN} impairs only Yvh1, but not Rei1 recruitment. Lsg1-TAP was co-transformed with plasmids each expressing copper-inducible Drg1 or Drg1^{DN} and galactose-inducible Nog1 or Nog1^{DN}, respectively. Cells were grown in raffinose-containing synthetic medium to early log phase and then supplemented with 0.5 mM copper sulphate and 2% galactose. After 3h, cells were lysed, the Lsg1-TAP particle was isolated and subjected to Western analyses using indicated

antibodies. **(B)** Indicated strains expressing Nog1^{DN} under control of GAL1 were treated with DMSO or Diazaborine to block Drg1 activity and visualized by fluorescence microscopy as in Figure 4. Scale bar = 5 μm. Quantification of the data is listed in Supplementary Table 2. **(C)** Rei1 binding site on the pre-60S clashes with Nog1-CTT:Rlp24 complex. Cryo-EM structures of Nog1-containing (PDB-3JCT) pre-60S and a Rei1-containing (PDB-6RZZ) pre-60S were superimposed. Release of Rlp24 allows recruitment of Rei1 to the pre-60S **(D)** Arx1 mislocalizes to the cytoplasm in *a rei1-TAP* mutant expressing NOG1^{DN}. The ARX1-GFP rei1Δ strain was transformed with either REI1 or rei1-TAP encoding plasmids under control of their natural promoter. Subsequently, the resultant strains were transformed with plasmids encoding galactose-inducible NOG1 or NOG1^{DN}, respectively. The transformants were grown in raffinose-containing medium to early log phase and then supplemented with 2% galactose. After 3h, cells were visualized by fluorescence microscopy. Scale bar = 5 μm. Quantification is listed in Supplementary File 3.

Figure 6. The Nog1-CTT:Rlp24 complex negatively regulates PET maturation. (A) Domain organization of Nog1 and Rlp24 showing interaction surfaces, and sites for truncation analyses. **(B)** Growth analysis of Nog1 truncations. *Left panel:* A Nog1 shuffle strain was transformed with the indicated constructs and spotted in 10-fold dilutions 5-FOA (SD) plates and incubated for 2-6 days at the indicated temperatures. *Right panel:* nog1Δ shuffle strain was transformed with the indicated plasmids. After shuffling out the *URA3-NOG1* plasmid on FOA-containing plates, strains were spotted in 10-fold serial dilutions on YPD plates and incubated for 2-4 days at the indicated temperatures. **(C)** Rlp24:Nog1 interactions contribute to early nucleolar/nuclear maturation. *Left panel:* BY wild-type cells were transformed with the indicated plasmids under control of the galactose-inducible GAL1 promoter and spotted in 10-fold dilutions on glucose- or galactose-containing media. Plates were incubated at 30°C for 2-4 days. *Right panel:* Mrt4-GFP, Arx1-GFP and Tif6-GFP strains were transformed with the indicated plasmids under control of GAL1 promoter. Cells were grown in raffinose-containing synthetic medium to early log phase and then supplemented with 2%

galactose. After 3h, cells were visualized by fluorescence microscopy. Scale bar = 5 μm. Quantification is listed in Supplementary File 3. **(D)** Drg1-mediated release of Rlp24 from Nog1 is required for PET assembly. Nog1 shuffle strains containing GFP tagged versions of assembly factors were transformed with Nog1 and $Nog1^{1-479}$ encoding plasmids. After shuffling out *URA3-NOG1* plasmid on 5-FOA, the resultant strains were grown in YPD and were treated with DMSO or Diazaborine (DIA) for 30 mins to inhibit Drg1-ATPase activity and the GFP tagged assembly factor was visualized by fluorescence microscopy. Scale bar = 5 μm. Quantification is listed in Supplementary File 3.

Figure 7. $Nog1^{DN}$ blocks the terminal cytoplasmic maturation steps. (A) $Nog1^{DN}$ impairs recycling of Mrt4 and Tif6. The *mrt4Δyvh1Δ* strain was co-transformed with plasmids encoding Mrt4-GFP or Mrt4G68E-GFP and Yvh1 or galactose-inducible $Nog1^{DN}$, respectively. To monitor Tif6 localization, the strain was co-transformed with plasmids encoding Tif6-GFP, Mrt4 or Mrt4G68E-GFP and Yvh1 or galactose-inducible $Nog1^{DN}$, respectively. Cells were grown in raffinose-containing synthetic medium to early log phase and then supplemented with 2% galactose. After 3h, cells were visualized by fluorescence microscopy. Scale bar = 5 μm. Quantification is listed in Supplementary File 3. **(B)** Mrt4G68E bypasses the need for YVH1, but does not rescue lethality associated with $Nog1^{DN}$ expression. The depicted strains were spotted in 10-fold dilutions on galactose-containing media and incubated at 30°C for 2-4 days. **(C)** $Nog1^{DN}$ impairs recruitment of Yvh1, but not release of the Mrt4-G68E gain-of-function mutant. A Lsg1-TAP mrt4Δ strain was co-transformed with plasmids encoding Mrt4 or Mrt4G68E and empty vector or galactose-inducible $Nog1^{DN}$, respectively. Cells were grown in raffinose-containing synthetic medium to early log phase and then supplemented with 2% galactose. After 3h, cells were lysed, purified through Lsg1-TAP and subjected to western analyses using indicated antibodies. **(D)** Nog1 release permits uL16 recruitment. Superimposition of cryo-EM structures of nuclear Nog1-containing pre-60S particle (PDB-3JCT) and uL16 on a mature 60S subunit (PDB-6R84) show how Nog1-NTD and G domain prevent recruitment of uL16 to the pre-60S.

Figure 8. A revised model for early cytoplasmic maturation of the pre-60S. Drg1 initiates the 60S cytoplasmic maturation pathway by binding to and releasing Rlp24 from the pre-60S bound Rlp24:Nog1-CTT complex and in an ATP-dependent manner (State I to State II). Removal of Rlp24 also releases its interacting partner Bud20, and consequently extracts the Nog1 C-terminal tail out of the polypeptide exit tunnel (PET) (State II). Extraction of Nog1-CTT from the PET, permits Rei1-CTT to probe PET integrity (State III). Successful Rei1-CTT insertion into the PET triggers ATP-dependent release of Arx1 by Ssa1/2 and Jjj1, concurrent Rei1 eviction (State III to State IV). This permits Reh1-CTT insertion into the PET (State IV). Nog1 release permits Yvh1 recruitment to evict Mrt4 and to initiate stalk assembly (State IV to State V). Nog1 eviction also permits eL40 and uL16 incorporation, and Nsa2 release. Stable uL16 accommodation into the pre-60S leads to Lsg1 mediating Nmd3 release, and thereby completing PET maturation. Nmd3 release triggers Reh1 release, and also licenses the GTPase Efl1 and co-factor Sdo1 to evict Tif6 (State V to State VI), thus driving a pre-60S towards translation competence.

Figure 2 – figure supplement 1. Co-enrichment of assembly factors with a maturing pre-60S subunit. 60S pre-ribosomes representing different maturation stages: nucleolar (Ssf1-TAP), nuclear (Rix1-TAP), nuclear and cytoplasmic (Arx1-TAP) and cytoplasmic (Lsg1-TAP) were purified and selected assembly factors were analyzed by Western blotting.

Legends to Supplementary Files

Supplementary File 1. List of yeast strains used in this study.

Supplementary File 2. List of plasmids used in this study.

Supplementary File 3. Quantification of microscopy data. The average fraction of >1000 cells showing stronger nuclear fluorescence than cytoplasmic (f_n) from three independent experiments is listed**.**

Acknowledgements

We thank M Peter, C Dargemont, A Johnson, M Fromont-Racine, B Stillman, F Lacroute, J Warner for generously sharing yeast strains and

antibodies. This work is dedicated to the memory of Dr. Cohue Peña, who unexpectedly passed away. We thank all members of the Panse laboratory for enthusiastic discussions. We thank the services of the Center for Microscopy and Image Analysis, University of Zurich for providing/maintaining imaging equipment.

Financial Disclosure

VGP is supported by grants from the Swiss National Science Foundation, NCCR RNA & Disease, Novartis Foundation, Olga Mayenfisch Stiftung and a Starting Grant from the European Research Council (EURIBIO260676). RA is supported by ERC grant Proteomics v3.0 (AdvG233226).

Conflict of interest

The authors declare that they have no conflict of interest.

References

ALTVATER, M., CHANG, Y., MELNIK, A., OCCHIPINTI, L., SCHUTZ, S., ROTHENBUSCH, U., PICOTTI, P. & PANSE, V. G. 2012. Targeted proteomics reveals compositional dynamics of 60S pre-ribosomes after nuclear export. *Mol Syst Biol,* 8**,** 628.

ALTVATER, M., SCHUTZ, S., CHANG, Y. & PANSE, V. G. 2014. Dissecting ribosome assembly and transport in budding yeast. *Methods Cell Biol,* 122**,** 437-61.

ASH, M. R., MAHER, M. J., MITCHELL GUSS, J. & JORMAKKA, M. 2012. The cation-dependent G-proteins: in a class of their own. *FEBS Lett,* 586**,** 2218-24.

BARRIO-GARCIA, C., THOMS, M., FLEMMING, D., KATER, L., BERNINGHAUSEN, O., BASSLER, J., BECKMANN, R. & HURT, E. 2016. Architecture of the Rix1-Rea1 checkpoint machinery during pre-60S-ribosome remodeling. *Nat Struct Mol Biol,* 23**,** 37-44.

BASSLER, J., KLEIN, I., SCHMIDT, C., KALLAS, M., THOMSON, E., WAGNER, M. A., BRADATSCH, B., RECHBERGER, G., STROHMAIER, H., HURT, E. & BERGLER, H. 2012. The conserved Bud20 zinc finger protein is a new component of the ribosomal 60S subunit export machinery. *Mol Cell Biol,* 32**,** 4898-912.

BEN-SHEM, A., GARREAU DE LOUBRESSE, N., MELNIKOV, S., JENNER, L., YUSUPOVA, G. & YUSUPOV, M. 2011. The structure of the eukaryotic ribosome at 3.0 A resolution. *Science,* 334**,** 1524-9.

BOURNE, H. R., SANDERS, D. A. & MCCORMICK, F. 1991. The GTPase superfamily: conserved structure and molecular mechanism. *Nature,* 349**,** 117-27.

BRADATSCH, B., LEIDIG, C., GRANNEMAN, S., GNÄDIG, M., TOLLERVEY, D., BÖTTCHER, B., BECKMANN, R. & HURT, E. 2012. Structure of the pre-60S ribosomal subunit with nuclear export factor Arx1 bound at the exit tunnel. *Nat Struct Mol Biol,* 19**,** 1234-1241.

COLLINS, B. C., GILLET, L. C., ROSENBERGER, G., ROST, H. L., VICHALKOVSKI, A., GSTAIGER, M. & AEBERSOLD, R. 2013. Quantifying protein interaction dynamics by SWATH mass spectrometry: application to the 14-3-3 system. *Nat Methods,* 10**,** 1246-53.

DONG, J., LAI, R., JENNINGS, J. L., LINK, A. J. & HINNEBUSCH, A. G. 2005. The novel ATP-binding cassette protein ARB1 is a shuttling factor that stimulates 40S and 60S ribosome biogenesis. *Mol Cell Biol,* 25**,** 9859-73.

ESCHER, C., REITER, L., MACLEAN, B., OSSOLA, R., HERZOG, F., CHILTON, J., MACCOSS, M. J. & RINNER, O. 2012. Using iRT, a normalized retention time for more targeted measurement of peptides. *Proteomics,* 12**,** 1111-21.

FAZA, M. B., CHANG, Y., OCCHIPINTI, L., KEMMLER, S. & PANSE, V. G. 2012. Role of Mex67-Mtr2 in the nuclear export of 40S pre-ribosomes. *PLoS Genet,* 8**,** e1002915.

FENG, B., MANDAVA, C. S., GUO, Q., WANG, J., CAO, W., LI, N., ZHANG, Y., ZHANG, Y., WANG, Z., WU, J., SANYAL, S., LEI, J. & GAO, N.

2014. Structural and functional insights into the mode of action of a universally conserved Obg GTPase. *PLoS Biol,* 12**,** e1001866.
FLEISCHER, T. C., WEAVER, C. M., MCAFEE, K. J., JENNINGS, J. L. & LINK, A. J. 2006. Systematic identification and functional screens of uncharacterized proteins associated with eukaryotic ribosomal complexes. *Genes Dev,* 20**,** 1294-307.
FORD, B., SKOWRONEK, K., BOYKEVISCH, S., BAR-SAGI, D. & NASSAR, N. 2005. Structure of the G60A mutant of Ras: implications for the dominant negative effect. *J Biol Chem,* 280**,** 25697-705.
GILLET, L. C., NAVARRO, P., TATE, S., ROST, H., SELEVSEK, N., REITER, L., BONNER, R. & AEBERSOLD, R. 2012. Targeted data extraction of the MS/MS spectra generated by data-independent acquisition: a new concept for consistent and accurate proteome analysis. *Mol Cell Proteomics,* 11**,** O111 016717.
GREBER, B. J., BOEHRINGER, D., MONTELLESE, C. & BAN, N. 2012. Cryo-EM structures of Arx1 and maturation factors Rei1 and Jjj1 bound to the 60S ribosomal subunit. *Nat Struct Mol Biol,* 19**,** 1228-33.
GREBER, B. J., GERHARDY, S., LEITNER, A., LEIBUNDGUT, M., SALEM, M., BOEHRINGER, D., LEULLIOT, N., AEBERSOLD, R., PANSE, V. G. & BAN, N. 2016. Insertion of the Biogenesis Factor Rei1 Probes the Ribosomal Tunnel during 60S Maturation. *Cell,* 164**,** 91-102.
HEDGES, J., WEST, M. & JOHNSON, A. W. 2005. Release of the export adapter, Nmd3p, from the 60S ribosomal subunit requires Rpl10p and the cytoplasmic GTPase Lsg1p. *EMBO J,* 24**,** 567-79.
JANKE, C., MAGIERA, M. M., RATHFELDER, N., TAXIS, C., REBER, S., MAEKAWA, H., MORENO-BORCHART, A., DOENGES, G., SCHWOB, E., SCHIEBEL, E. & KNOP, M. 2004. A versatile toolbox for PCR-based tagging of yeast genes: new fluorescent proteins, more markers and promoter substitution cassettes. *Yeast,* 21**,** 947-62.
JENSEN, B. C., WANG, Q., KIFER, C. T. & PARSONS, M. 2003. The NOG1 GTP-binding protein is required for biogenesis of the 60 S ribosomal subunit. *J Biol Chem,* 278**,** 32204-11.
KALLSTROM, G., HEDGES, J. & JOHNSON, A. 2003. The putative GTPases Nog1p and Lsg1p are required for 60S ribosomal subunit biogenesis and are localized to the nucleus and cytoplasm, respectively. *Mol Cell Biol,* 23**,** 4344-55.
KAPPEL, L., LOIBL, M., ZISSER, G., KLEIN, I., FRUHMANN, G., GRUBER, C., UNTERWEGER, S., RECHBERGER, G., PERTSCHY, B. & BERGLER, H. 2012. Rlp24 activates the AAA-ATPase Drg1 to initiate cytoplasmic pre-60S maturation. *J Cell Biol,* 199**,** 771-82.
KARGAS, V., CASTRO-HARTMANN, P., ESCUDERO-URQUIJO, N., DENT, K., HILCENKO, C., SAILER, C., ZISSER, G., MARQUES-CARVALHO, M. J., PELLEGRINO, S., WAWIORKA, L., FREUND, S. M., WAGSTAFF, J. L., ANDREEVA, A., FAILLE, A., CHEN, E., STENGEL, F., BERGLER, H. & WARREN, A. J. 2019. Mechanism of completion of peptidyltransferase centre assembly in eukaryotes. *Elife,* 8.
KATER, L., THOMS, M., BARRIO-GARCIA, C., CHENG, J., ISMAIL, S., AHMED, Y. L., BANGE, G., KRESSLER, D., BERNINGHAUSEN, O., SINNING, I., HURT, E. & BECKMANN, R. 2017. Visualizing the

Assembly Pathway of Nucleolar Pre-60S Ribosomes. *Cell,* 171**,** 1599-1610 e14.
KELLER, A., NESVIZHSKII, A. I., KOLKER, E. & AEBERSOLD, R. 2002. Empirical statistical model to estimate the accuracy of peptide identifications made by MS/MS and database search. *Anal Chem,* 74**,** 5383-92.
KEMMLER, S., OCCHIPINTI, L., VEISU, M. & PANSE, V. G. 2009. Yvh1 is required for a late maturation step in the 60S biogenesis pathway. *J Cell Biol,* 186**,** 863-80.
KRESSLER, D., HURT, E. & BASSLER, J. 2017. A Puzzle of Life: Crafting Ribosomal Subunits. *Trends Biochem Sci,* 42**,** 640-654.
KRESSLER, D., HURT, E., BERGLER, H. & BASSLER, J. 2012. The power of AAA-ATPases on the road of pre-60S ribosome maturation--molecular machines that strip pre-ribosomal particles. *Biochim Biophys Acta,* 1823**,** 92-100.
KRESSLER, D., ROSER, D., PERTSCHY, B. & HURT, E. 2008. The AAA ATPase Rix7 powers progression of ribosome biogenesis by stripping Nsa1 from pre-60S particles. *J Cell Biol,* 181**,** 935-44.
LAM, H., DEUTSCH, E. W., EDDES, J. S., ENG, J. K., STEIN, S. E. & AEBERSOLD, R. 2008. Building consensus spectral libraries for peptide identification in proteomics. *Nat Methods,* 5**,** 873-5.
LAMBERT, J. P., IVOSEV, G., COUZENS, A. L., LARSEN, B., TAIPALE, M., LIN, Z. Y., ZHONG, Q., LINDQUIST, S., VIDAL, M., AEBERSOLD, R., PAWSON, T., BONNER, R., TATE, S. & GINGRAS, A. C. 2013. Mapping differential interactomes by affinity purification coupled with data-independent mass spectrometry acquisition. *Nat Methods,* 10**,** 1239-45.
LAPIK, Y. R., MISRA, J. M., LAU, L. F. & PESTOV, D. G. 2007. Restricting conformational flexibility of the switch II region creates a dominant-inhibitory phenotype in Obg GTPase Nog1. *Mol Cell Biol,* 27**,** 7735-44.
LEBRETON, A., SAVEANU, C., DECOURTY, L., RAIN, J. C., JACQUIER, A. & FROMONT-RACINE, M. 2006. A functional network involved in the recycling of nucleocytoplasmic pre-60S factors. *J Cell Biol,* 173**,** 349-60.
LO, K. Y., LI, Z., BUSSIERE, C., BRESSON, S., MARCOTTE, E. M. & JOHNSON, A. W. 2010. Defining the pathway of cytoplasmic maturation of the 60S ribosomal subunit. *Mol Cell,* 39**,** 196-208.
LO, K. Y., LI, Z., WANG, F., MARCOTTE, E. M. & JOHNSON, A. W. 2009. Ribosome stalk assembly requires the dual-specificity phosphatase Yvh1 for the exchange of Mrt4 with P0. *J Cell Biol,* 186**,** 849-62.
LOIBL, M., KLEIN, I., PRATTES, M., SCHMIDT, C., KAPPEL, L., ZISSER, G., GUNGL, A., KRIEGER, E., PERTSCHY, B. & BERGLER, H. 2014. The drug diazaborine blocks ribosome biogenesis by inhibiting the AAA-ATPase Drg1. *J Biol Chem,* 289**,** 3913-22.
LONGTINE, M. S., MCKENZIE, A., 3RD, DEMARINI, D. J., SHAH, N. G., WACH, A., BRACHAT, A., PHILIPPSEN, P. & PRINGLE, J. R. 1998. Additional modules for versatile and economical PCR-based gene deletion and modification in Saccharomyces cerevisiae. *Yeast,* 14**,** 953-61.

MA, C., WU, S., LI, N., CHEN, Y., YAN, K., LI, Z., ZHENG, L., LEI, J., WOOLFORD, J. L., JR. & GAO, N. 2017. Structural snapshot of cytoplasmic pre-60S ribosomal particles bound by Nmd3, Lsg1, Tif6 and Reh1. *Nat Struct Mol Biol,* 24**,** 214-220.

MALYUTIN, A. G., MUSALGAONKAR, S., PATCHETT, S., FRANK, J. & JOHNSON, A. W. 2017. Nmd3 is a structural mimic of eIF5A, and activates the cpGTPase Lsg1 during 60S ribosome biogenesis. *EMBO J,* 36**,** 854-868.

MATSUO, Y., GRANNEMAN, S., THOMS, M., MANIKAS, R. G., TOLLERVEY, D. & HURT, E. 2014. Coupled GTPase and remodelling ATPase activities form a checkpoint for ribosome export. *Nature,* 505**,** 112-6.

MEYER, A. E., HOOVER, L. A. & CRAIG, E. A. 2010. The cytosolic J-protein, Jjj1, and Rei1 function in the removal of the pre-60 S subunit factor Arx1. *J Biol Chem,* 285**,** 961-8.

MEYER, A. E., HUNG, N. J., YANG, P., JOHNSON, A. W. & CRAIG, E. A. 2007. The specialized cytosolic J-protein, Jjj1, functions in 60S ribosomal subunit biogenesis. *Proc Natl Acad Sci U S A,* 104**,** 1558-63.

NAVARRO, P., KUHAREV, J., GILLET, L. C., BERNHARDT, O. M., MACLEAN, B., ROST, H. L., TATE, S. A., TSOU, C. C., REITER, L., DISTLER, U., ROSENBERGER, G., PEREZ-RIVEROL, Y., NESVIZHSKII, A. I., AEBERSOLD, R. & TENZER, S. 2016. A multicenter study benchmarks software tools for label-free proteome quantification. *Nat Biotechnol,* 34**,** 1130-1136.

NERURKAR, P., ALTVATER, M., GERHARDY, S., SCHUTZ, S., FISCHER, U., WEIRICH, C. & PANSE, V. G. 2015. Eukaryotic Ribosome Assembly and Nuclear Export. *Int Rev Cell Mol Biol,* 319**,** 107-40.

NISSAN, T. A., BASSLER, J., PETFALSKI, E., TOLLERVEY, D. & HURT, E. 2002. 60S pre-ribosome formation viewed from assembly in the nucleolus until export to the cytoplasm. *EMBO J,* 21**,** 5539-47.

PARNELL, K. M. & BASS, B. L. 2009. Functional redundancy of yeast proteins Reh1 and Rei1 in cytoplasmic 60S subunit maturation. *Mol Cell Biol,* 29**,** 4014-23.

PAUSCH, P., SINGH, U., AHMED, Y. L., PILLET, B., MURAT, G., ALTEGOER, F., STIER, G., THOMS, M., HURT, E., SINNING, I., BANGE, G. & KRESSLER, D. 2015. Co-translational capturing of nascent ribosomal proteins by their dedicated chaperones. *Nat Commun,* 6**,** 7494.

PENA, C., HURT, E. & PANSE, V. G. 2017. Eukaryotic ribosome assembly, transport and quality control. *Nat Struct Mol Biol,* 24**,** 689-699.

PERTSCHY, B., SAVEANU, C., ZISSER, G., LEBRETON, A., TENGG, M., JACQUIER, A., LIEBMINGER, E., NOBIS, B., KAPPEL, L., VAN DER KLEI, I., HOGENAUER, G., FROMONT-RACINE, M. & BERGLER, H. 2007. Cytoplasmic recycling of 60S preribosomal factors depends on the AAA protein Drg1. *Mol Cell Biol,* 27**,** 6581-92.

PICOTTI, P. & AEBERSOLD, R. 2012. Selected reaction monitoring-based proteomics: workflows, potential, pitfalls and future directions. *Nat Methods,* 9**,** 555-66.

PUIG, O., CASPARY, F., RIGAUT, G., RUTZ, B., BOUVERET, E., BRAGADO-NILSSON, E., WILM, M. & SERAPHIN, B. 2001. The

tandem affinity purification (TAP) method: a general procedure of protein complex purification. *Methods,* 24**,** 218-29.

REITER, L., CLAASSEN, M., SCHRIMPF, S. P., JOVANOVIC, M., SCHMIDT, A., BUHMANN, J. M., HENGARTNER, M. O. & AEBERSOLD, R. 2009. Protein identification false discovery rates for very large proteomics data sets generated by tandem mass spectrometry. *Mol Cell Proteomics,* 8**,** 2405-17.

ROST, H. L., LIU, Y., D'AGOSTINO, G., ZANELLA, M., NAVARRO, P., ROSENBERGER, G., COLLINS, B. C., GILLET, L., TESTA, G., MALMSTROM, L. & AEBERSOLD, R. 2016. TRIC: an automated alignment strategy for reproducible protein quantification in targeted proteomics. *Nat Methods,* 13**,** 777-83.

ROST, H. L., ROSENBERGER, G., NAVARRO, P., GILLET, L., MILADINOVIC, S. M., SCHUBERT, O. T., WOLSKI, W., COLLINS, B. C., MALMSTROM, J., MALMSTROM, L. & AEBERSOLD, R. 2014. OpenSWATH enables automated, targeted analysis of data-independent acquisition MS data. *Nat Biotechnol,* 32**,** 219-23.

SANGHAI, Z. A., MILLER, L., MOLLOY, K. R., BARANDUN, J., HUNZIKER, M., CHAKER-MARGOT, M., WANG, J., CHAIT, B. T. & KLINGE, S. 2018. Modular assembly of the nucleolar pre-60S ribosomal subunit. *Nature,* 556**,** 126-129.

SAVEANU, C., NAMANE, A., GLEIZES, P. E., LEBRETON, A., ROUSSELLE, J. C., NOAILLAC-DEPEYRE, J., GAS, N., JACQUIER, A. & FROMONT-RACINE, M. 2003. Sequential protein association with nascent 60S ribosomal particles. *Mol Cell Biol,* 23**,** 4449-60.

SCHUBERT, O. T., GILLET, L. C., COLLINS, B. C., NAVARRO, P., ROSENBERGER, G., WOLSKI, W. E., LAM, H., AMODEI, D., MALLICK, P., MACLEAN, B. & AEBERSOLD, R. 2015. Building high-quality assay libraries for targeted analysis of SWATH MS data. *Nat Protoc,* 10**,** 426-41.

SENGUPTA, J., BUSSIERE, C., PALLESEN, J., WEST, M., JOHNSON, A. W. & FRANK, J. 2010. Characterization of the nuclear export adaptor protein Nmd3 in association with the 60S ribosomal subunit. *J Cell Biol,* 189**,** 1079-86.

SHTEYNBERG, D., DEUTSCH, E. W., LAM, H., ENG, J. K., SUN, Z., TASMAN, N., MENDOZA, L., MORITZ, R. L., AEBERSOLD, R. & NESVIZHSKII, A. I. 2011. iProphet: multi-level integrative analysis of shotgun proteomic data improves peptide and protein identification rates and error estimates. *Mol Cell Proteomics,* 10**,** M111 007690.

SU, T., IZAWA, T., THOMS, M., YAMASHITA, Y., CHENG, J., BERNINGHAUSEN, O., HARTL, F. U., INADA, T., NEUPERT, W. & BECKMANN, R. 2019. Structure and function of Vms1 and Arb1 in RQC and mitochondrial proteome homeostasis. *Nature,* 570**,** 538-542.

TELEMAN, J., ROST, H. L., ROSENBERGER, G., SCHMITT, U., MALMSTROM, L., MALMSTROM, J. & LEVANDER, F. 2015. DIANA--algorithmic improvements for analysis of data-independent acquisition MS data. *Bioinformatics,* 31**,** 555-62.

WEIS, F., GIUDICE, E., CHURCHER, M., JIN, L., HILCENKO, C., WONG, C. C., TRAYNOR, D., KAY, R. R. & WARREN, A. J. 2015. Mechanism of

eIF6 release from the nascent 60S ribosomal subunit. *Nat Struct Mol Biol,* 22**,** 914-9.
WU, S., TUTUNCUOGLU, B., YAN, K., BROWN, H., ZHANG, Y., TAN, D., GAMALINDA, M., YUAN, Y., LI, Z., JAKOVLJEVIC, J., MA, C., LEI, J., DONG, M. Q., WOOLFORD, J. L., JR. & GAO, N. 2016. Diverse roles of assembly factors revealed by structures of late nuclear pre-60S ribosomes. *Nature,* 534**,** 133-7.
ZHOU, Y., MUSALGAONKAR, S., JOHNSON, A. W. & TAYLOR, D. W. 2019. Tightly-orchestrated rearrangements govern catalytic center assembly of the ribosome. *Nat Commun,* 10**,** 958.
ZISSER, G., OHMAYER, U., MAUERHOFER, C., MITTERER, V., KLEIN, I., RECHBERGER, G. N., WOLINSKI, H., PRATTES, M., PERTSCHY, B., MILKEREIT, P. & BERGLER, H. 2018. Viewing pre-60S maturation at a minute's timescale. *Nucleic Acids Res,* 46**,** 3140-3151.

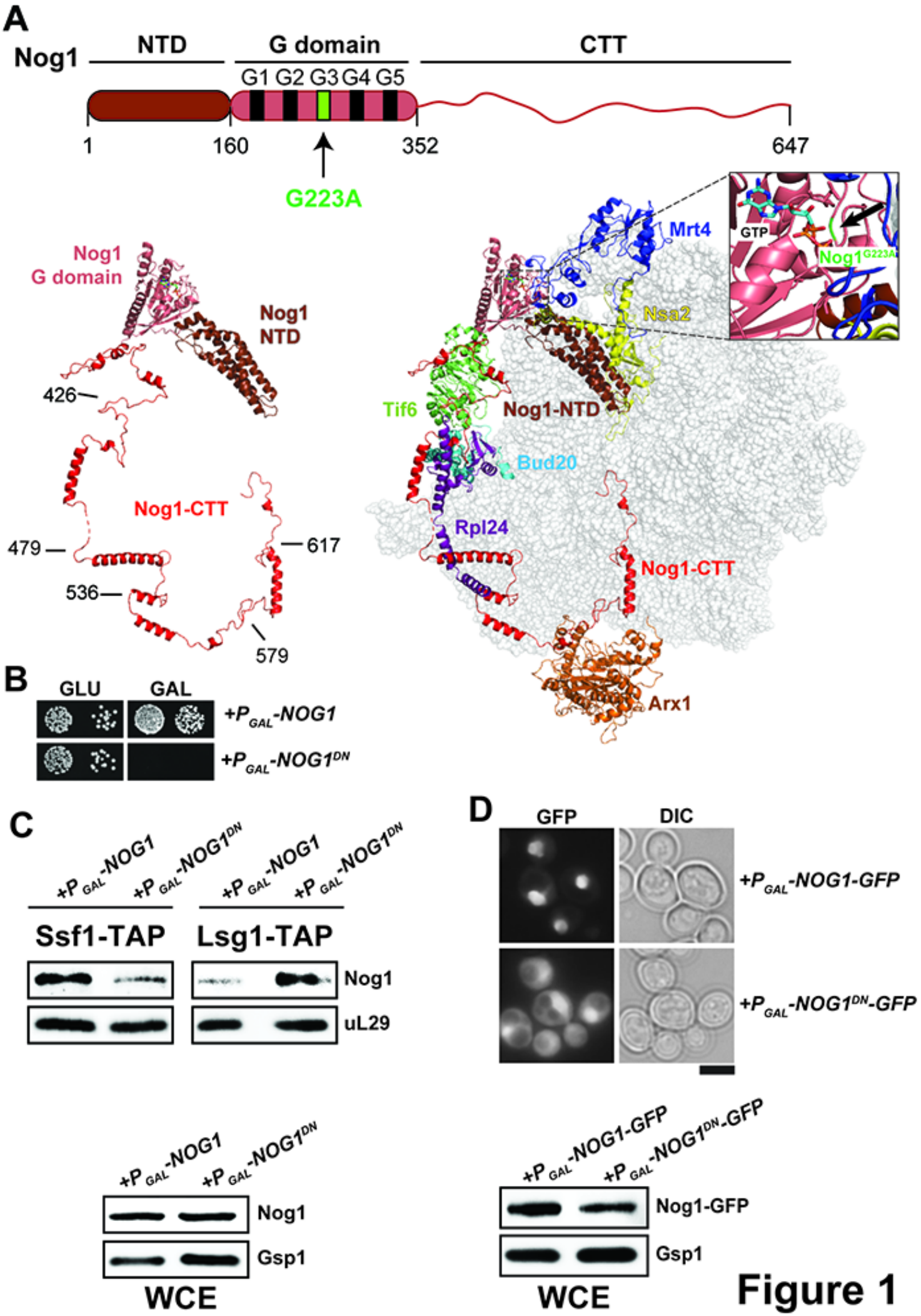
A
Nog1
NTD
G domain
CTT
G1 G2 G3 G4 G5
1
160
352
647
G223A
Nog1
G domain
Nog1
NTD
426
Nog1-CTT
479
617
536
579
Mrt4
GTP
Nog1G223A
Nsa2
Tif6
Nog1-NTD
Bud20
Rpl24
Nog1-CTT
Arx1
B
GLU
GAL
+PGAL-NOG1
+PGAL-NOG1DN
C
+PGAL-NOG1
+PGAL-NOG1DN
+PGAL-NOG1
+PGAL-NOG1DN
Ssf1-TAP
Lsg1-TAP
Nog1
uL29
D
GFP
DIC
+PGAL-NOG1-GFP
+PGAL-NOG1DN-GFP
+PGAL-NOG1
+PGAL-NOG1DN
Nog1
Gsp1
WCE
+PGAL-NOG1-GFP
+PGAL-NOG1DN-GFP
Nog1-GFP
Gsp1
WCE

Figure 1

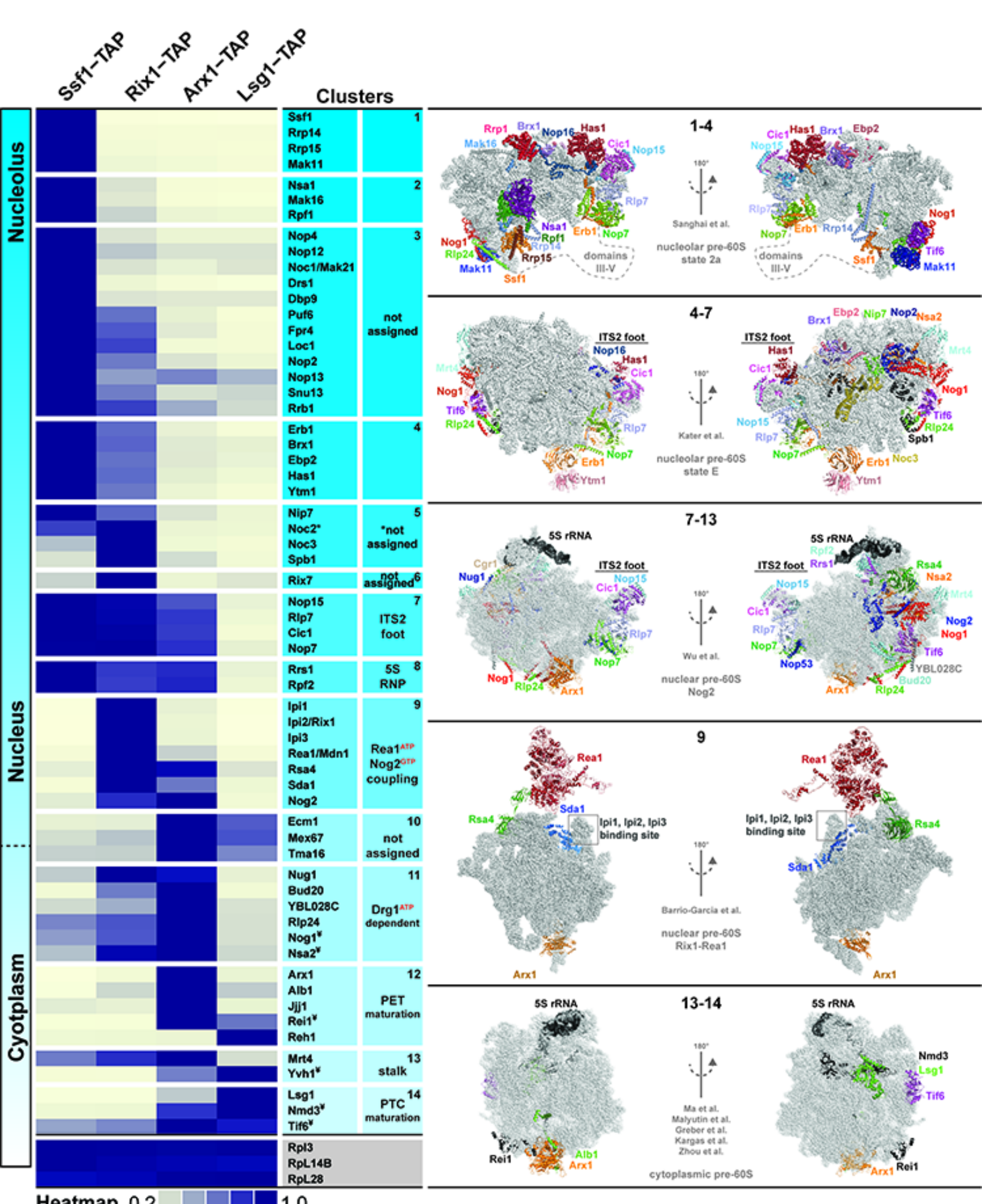
Ssf1-TAP
Rix1-TAP
Arx1-TAP
Lsg1-TAP
Clusters
Nucleolus
Nucleus
Cytoplasm
Ssf1
Rrp14
Rrp15
Mak11
1
Nsa1
Mak16
Rpf1
2
Nop4
Nop12
Noc1/Mak21
Drs1
Dbp9
Puf6
Fpr4
Loc1
Nop2
Nop13
Snu13
Rrb1
not assigned
3
Erb1
Brx1
Ebp2
Has1
Ytm1
4
Nip7
Noc2*
Noc3
Spb1
*not assigned
5
Rix7
not assigned
6
Nop15
Rlp7
Cic1
Nop7
ITS2 foot
7
Rrs1
Rpf2
5S RNP
8
Ipi1
Ipi2/Rix1
Ipi3
Rea1/Mdn1
Rsa4
Sda1
Nog2
Rea1ATP Nog2GTP coupling
9
Ecm1
Mex67
Tma16
not assigned
10
Nug1
Bud20
YBL028C
Rlp24
Nog1¥
Nsa2¥
Drg1ATP dependent
11
Arx1
Alb1
Jjj1
Rei1¥
Reh1
PET maturation
12
Mrt4
Yvh1¥
stalk
13
Lsg1
Nmd3¥
Tif6¥
PTC maturation
14
Rpl3
RpL14B
RpL28
Heatmap 0.2 1.0
1-4
Sanghai et al.
nucleolar pre-60S state 2a
domains III-V
4-7
Kater et al.
nucleolar pre-60S state E
ITS2 foot
7-13
Wu et al.
nuclear pre-60S Nog2
5S rRNA
9
Barrio-Garcia et al.
nuclear pre-60S Rix1-Rea1
Rea1
Sda1
Rsa4
Arx1
Ipi1, Ipi2, Ipi3 binding site
13-14
Ma et al.
Malyutin et al.
Greber et al.
Kargas et al.
Zhou et al.
cytoplasmic pre-60S
Nmd3
Lsg1
Tif6
Rei1
Alb1

Figure 2

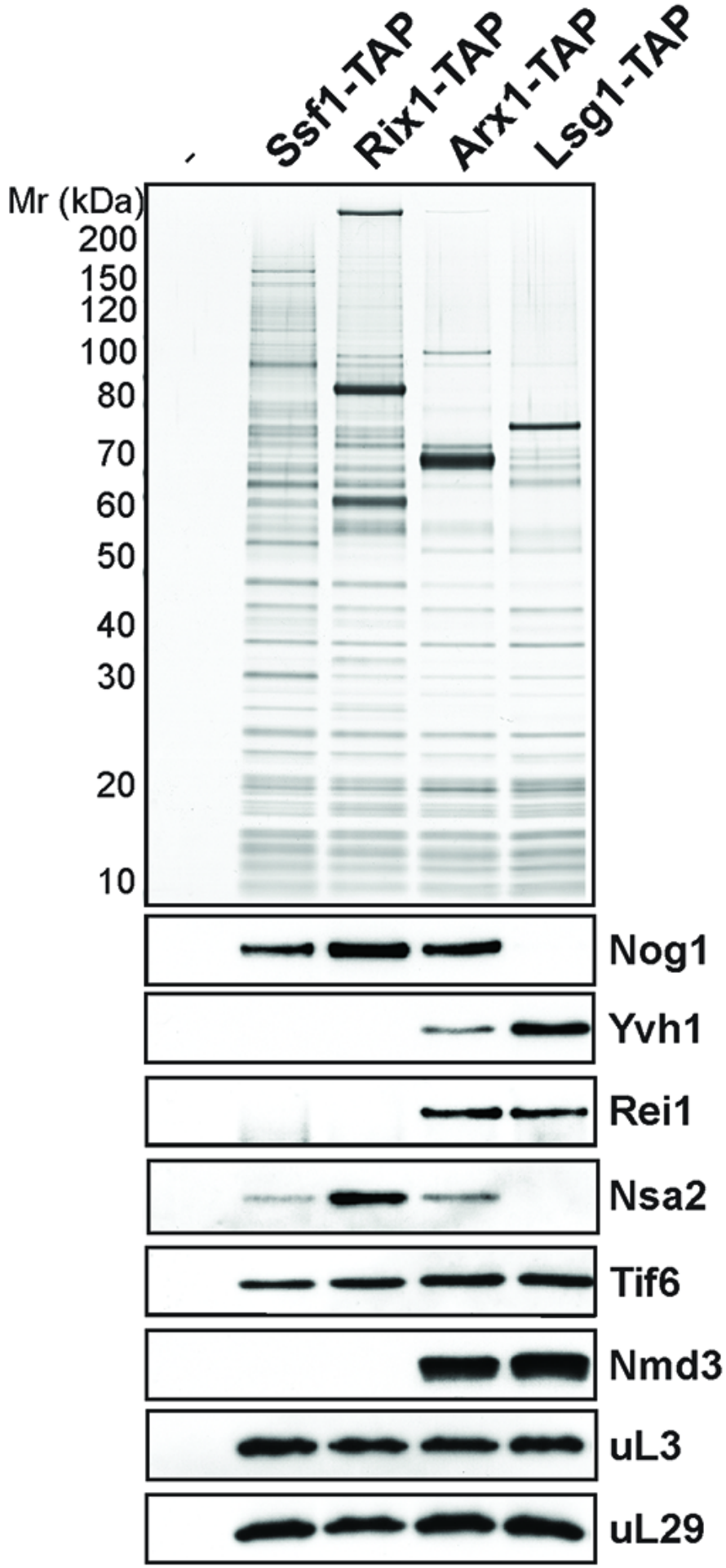

Figure 2- figure supplement 1

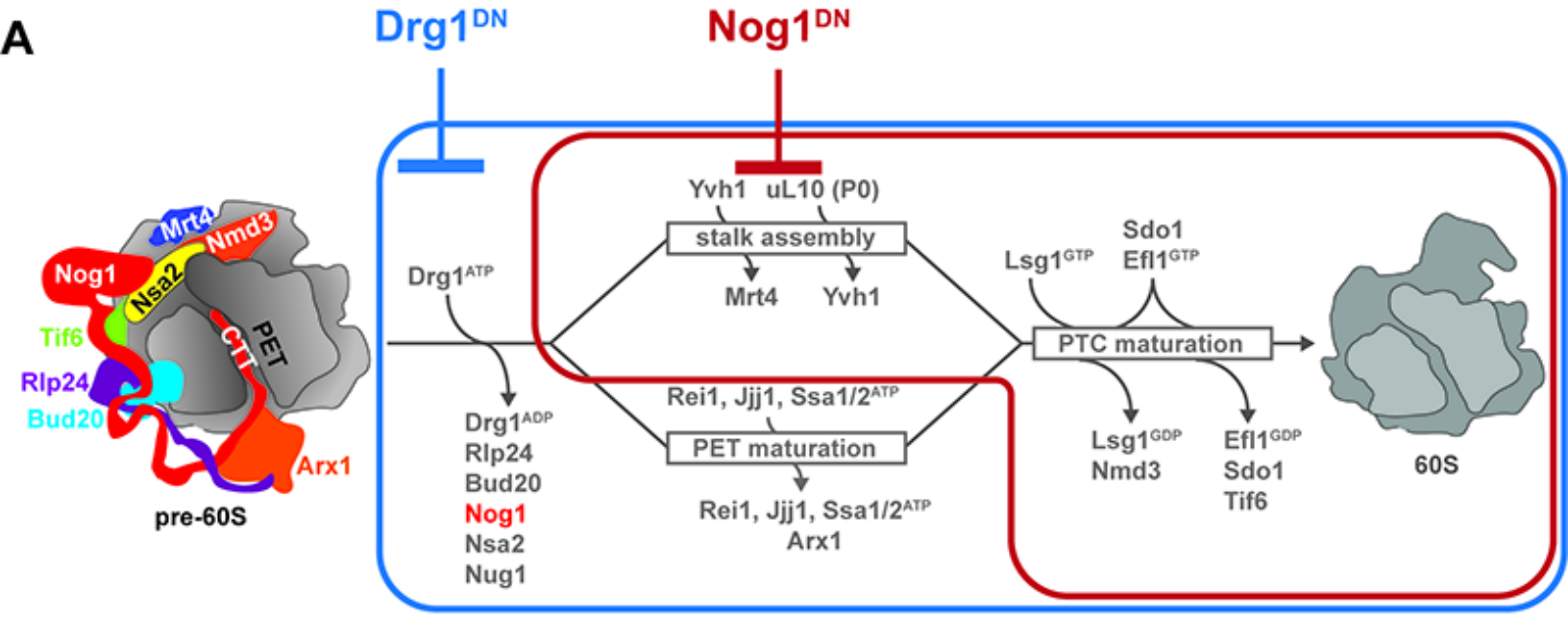
A
Drg1DN
Nog1DN
Mrt4
Nmd3
Nog1
Nsa2
Tif6
Rlp24
Bud20
PET
CTT
Arx1
pre-60S
Yvh1 uL10 (P0)
stalk assembly
Mrt4 Yvh1
Drg1ATP
Drg1ADP
Rlp24
Bud20
Nog1
Nsa2
Nug1
Rei1, Jjj1, Ssa1/2ATP
PET maturation
Rei1, Jjj1, Ssa1/2ATP
Arx1
Lsg1GTP
Sdo1
Efl1GTP
PTC maturation
Lsg1GDP
Nmd3
Efl1GDP
Sdo1
Tif6
60S

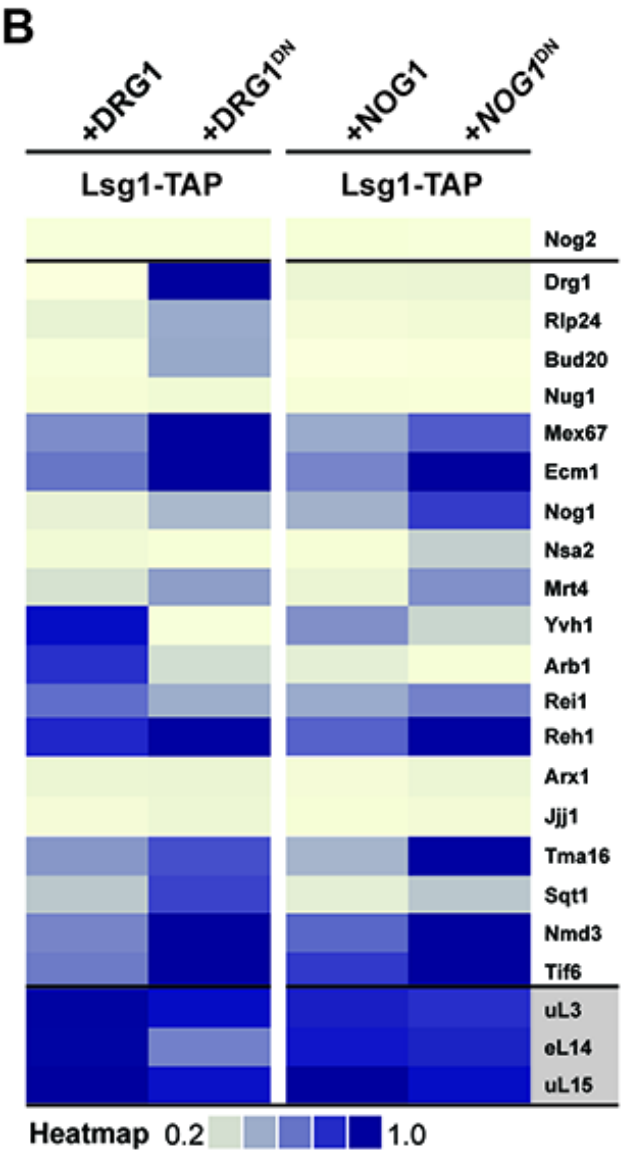
B
+DRG1
+DRG1DN
+NOG1
+NOG1DN
Lsg1-TAP
Lsg1-TAP
Nog2
Drg1
Rlp24
Bud20
Nug1
Mex67
Ecm1
Nog1
Nsa2
Mrt4
Yvh1
Arb1
Rei1
Reh1
Arx1
Jjj1
Tma16
Sqt1
Nmd3
Tif6
uL3
eL14
uL15
Heatmap 0.2
1.0

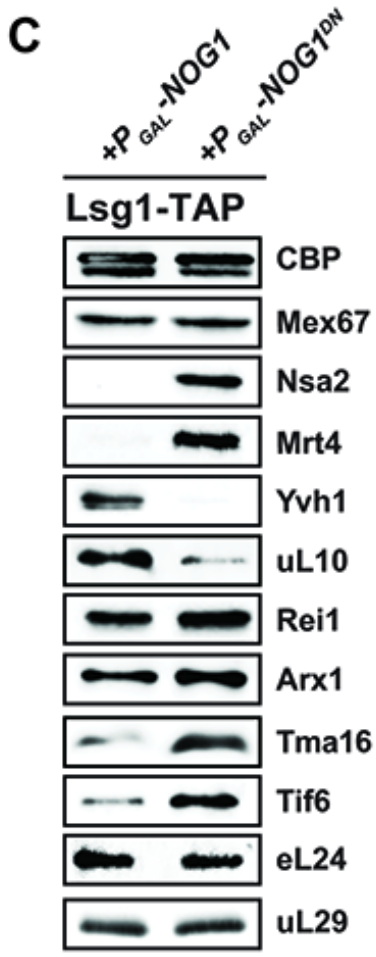
C
+PGAL-NOG1
+PGAL-NOG1DN
Lsg1-TAP
CBP
Mex67
Nsa2
Mrt4
Yvh1
uL10
Rei1
Arx1
Tma16
Tif6
eL24
uL29

Figure 3

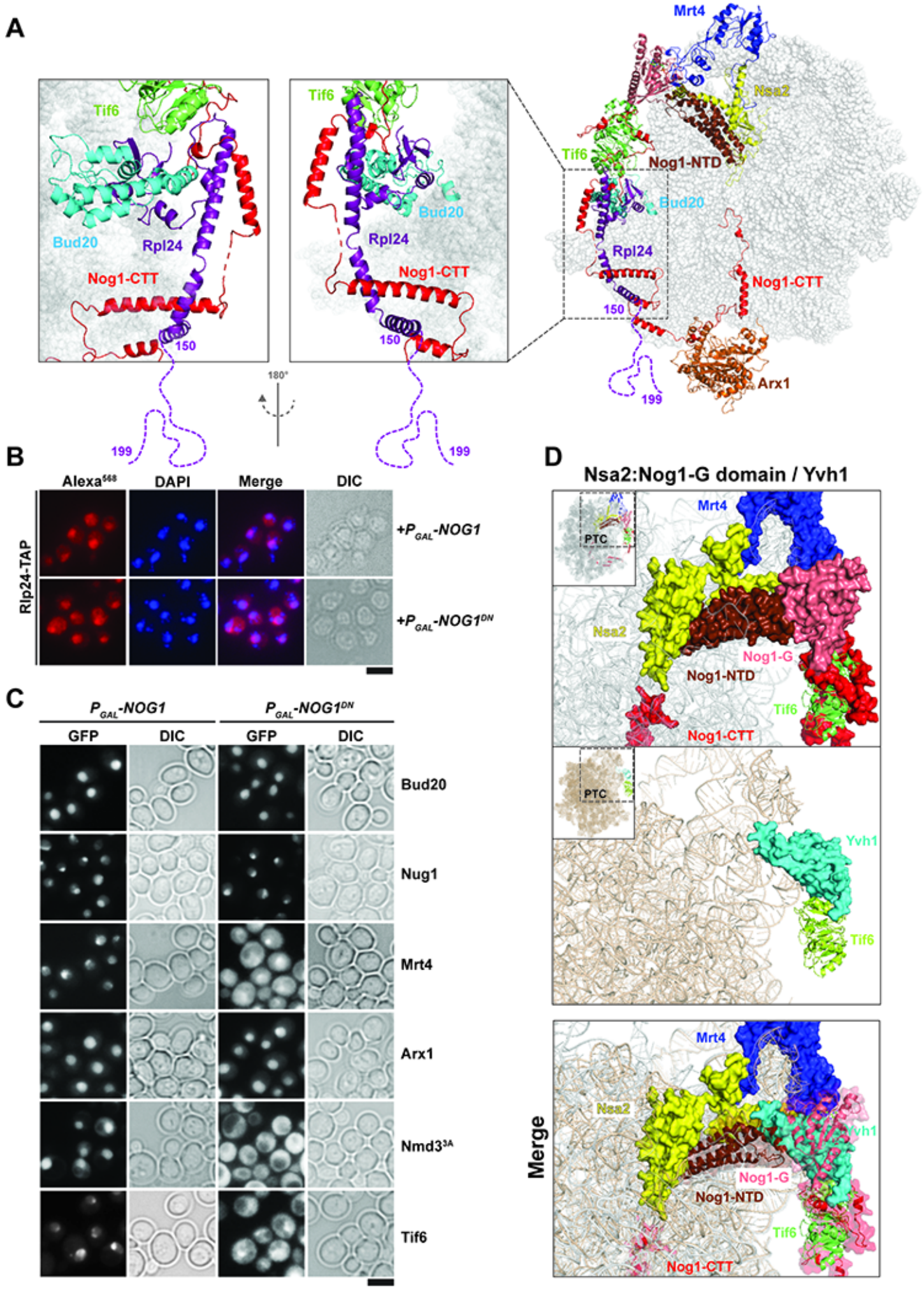
A
Mrt4
Nsa2
Tif6
Nog1-NTD
Bud20
Rpl24
Nog1-CTT
150
199
Arx1
180°
B
Alexa568
DAPI
Merge
DIC
Rlp24-TAP
+P GAL -NOG1
+P GAL -NOG1 DN
C
P GAL -NOG1
P GAL -NOG1 DN
GFP
DIC
Bud20
Nug1
Mrt4
Arx1
Nmd3 3A
Tif6
D
Nsa2:Nog1-G domain / Yvh1
PTC
Nog1-G
Yvh1
Merge

Figure 4

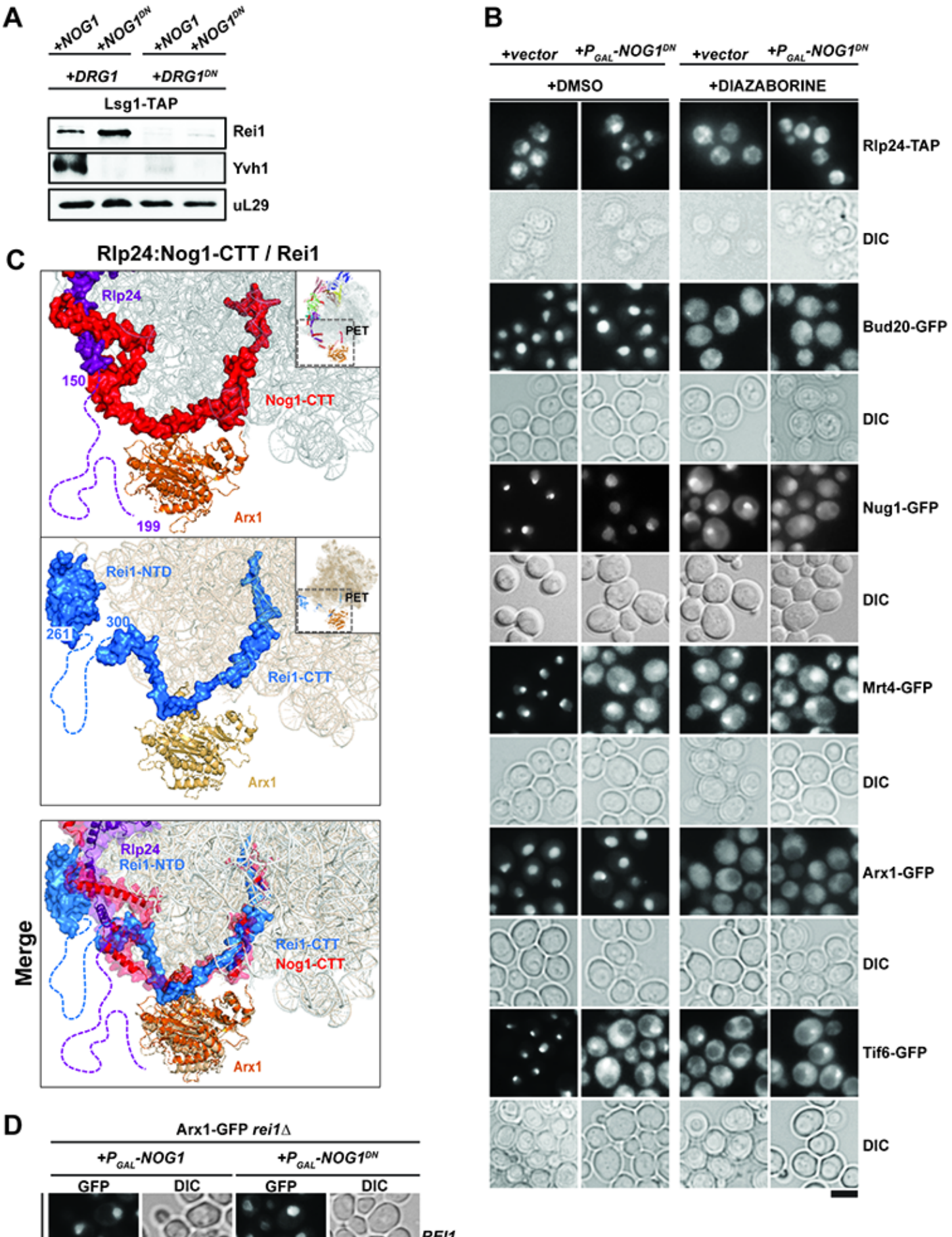
A
+NOG1
+NOG1DN
+NOG1
+NOG1DN
+DRG1
+DRG1DN
Lsg1-TAP
Rei1
Yvh1
uL29
B
+vector
+PGAL-NOG1DN
+vector
+PGAL-NOG1DN
+DMSO
+DIAZABORINE
Rlp24-TAP
DIC
Bud20-GFP
DIC
Nug1-GFP
DIC
Mrt4-GFP
DIC
Arx1-GFP
DIC
Tif6-GFP
DIC
C
Rlp24:Nog1-CTT / Rei1
Rlp24
PET
150
Nog1-CTT
199
Arx1
Rei1-NTD
PET
261
300
Rei1-CTT
Arx1
Merge
Rlp24
Rei1-NTD
Rei1-CTT
Nog1-CTT
Arx1
D
Arx1-GFP rei1Δ
+PGAL-NOG1
+PGAL-NOG1DN
GFP
DIC
GFP
DIC
Arx1-GFP
REI1
Rei1-TAP

Figure 5

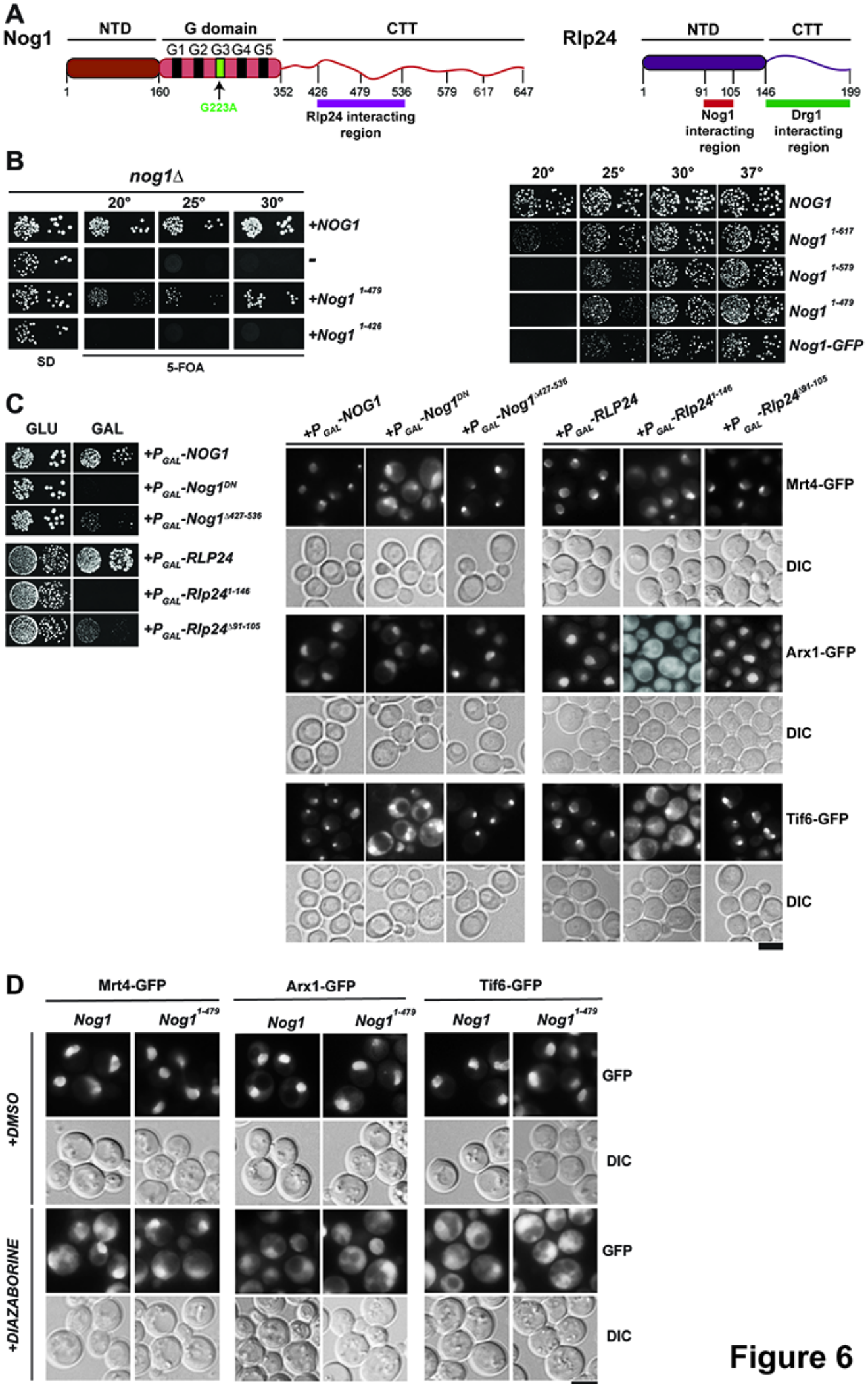
A
Nog1
NTD
G domain
G1 G2 G3 G4 G5
CTT
1
160
G223A
352
426
479
536
579
617
647
Rlp24 interacting region
Rlp24
NTD
CTT
1
91
105
146
199
Nog1 interacting region
Drg1 interacting region
B
nog1Δ
20°
25°
30°
+NOG1
-
+Nog1 1-479
+Nog1 1-426
SD
5-FOA
20°
25°
30°
37°
NOG1
Nog1 1-617
Nog1 1-579
Nog1 1-479
Nog1-GFP
C
GLU
GAL
+P GAL-NOG1
+P GAL-Nog1 DN
+P GAL-Nog1 Δ427-536
+P GAL-RLP24
+P GAL-Rlp24 1-146
+P GAL-Rlp24 Δ91-105
+P GAL-NOG1
+P GAL-Nog1 DN
+P GAL-Nog1 Δ427-536
+P GAL-RLP24
+P GAL-Rlp24 1-146
+P GAL-Rlp24 Δ91-105
Mrt4-GFP
DIC
Arx1-GFP
DIC
Tif6-GFP
DIC
D
Mrt4-GFP
Arx1-GFP
Tif6-GFP
Nog1
Nog1 1-479
Nog1
Nog1 1-479
Nog1
Nog1 1-479
+DMSO
+DIAZABORINE
GFP
DIC
GFP
DIC

Figure 6

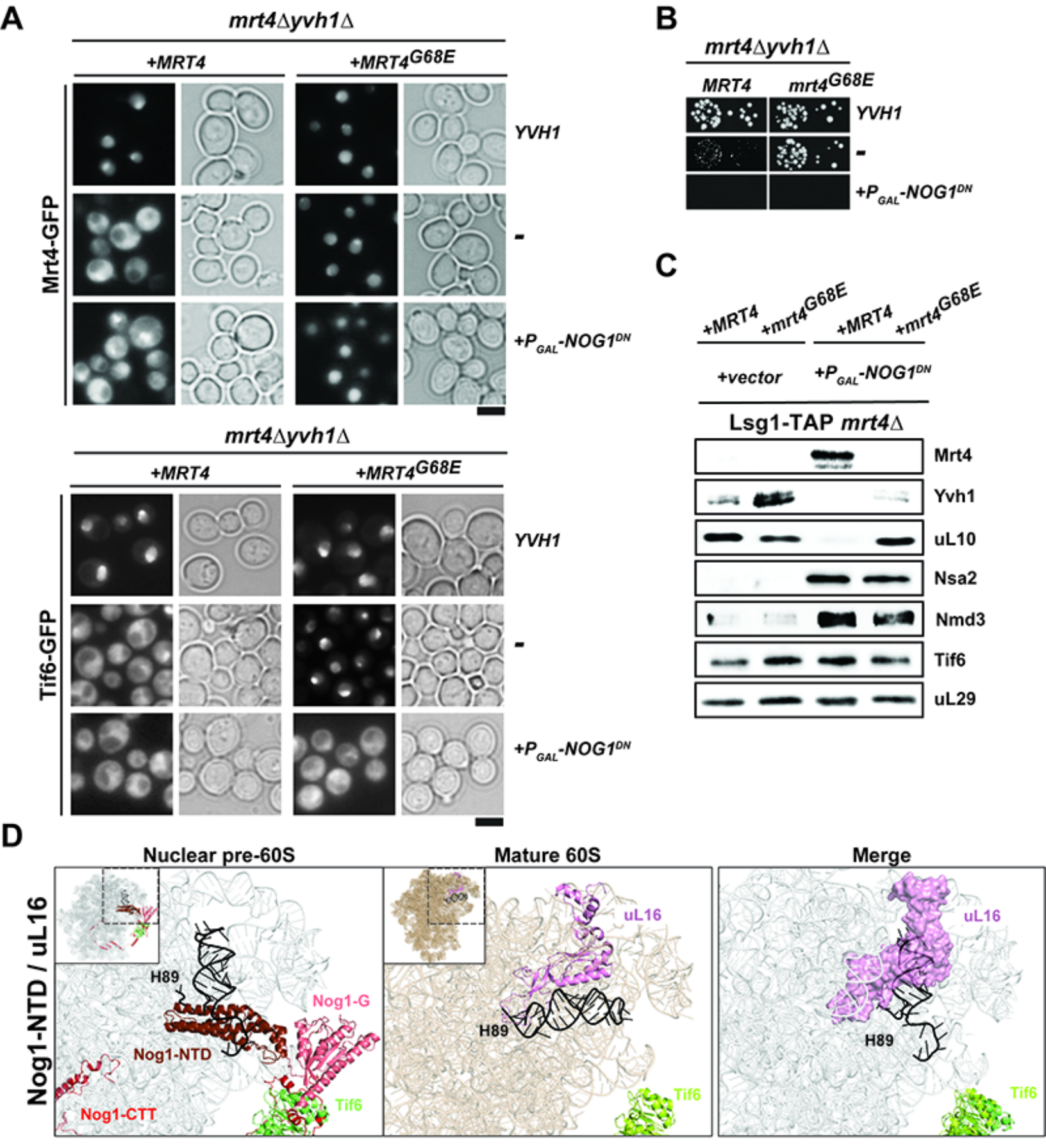
A
mrt4Δyvh1Δ
+MRT4
+MRT4G68E
Mrt4-GFP
YVH1
-
+PGAL-NOG1DN
mrt4Δyvh1Δ
+MRT4
+MRT4G68E
Tif6-GFP
YVH1
-
+PGAL-NOG1DN
B
mrt4Δyvh1Δ
MRT4
mrt4G68E
YVH1
-
+PGAL-NOG1DN
C
+MRT4
+mrt4G68E
+MRT4
+mrt4G68E
+vector
+PGAL-NOG1DN
Lsg1-TAP mrt4Δ
Mrt4
Yvh1
uL10
Nsa2
Nmd3
Tif6
uL29
D
Nuclear pre-60S
Mature 60S
Merge
Nog1-NTD / uL16
H89
Nog1-G
Nog1-NTD
Nog1-CTT
Tif6
uL16
H89
Tif6
uL16
H89
Tif6

Figure 7

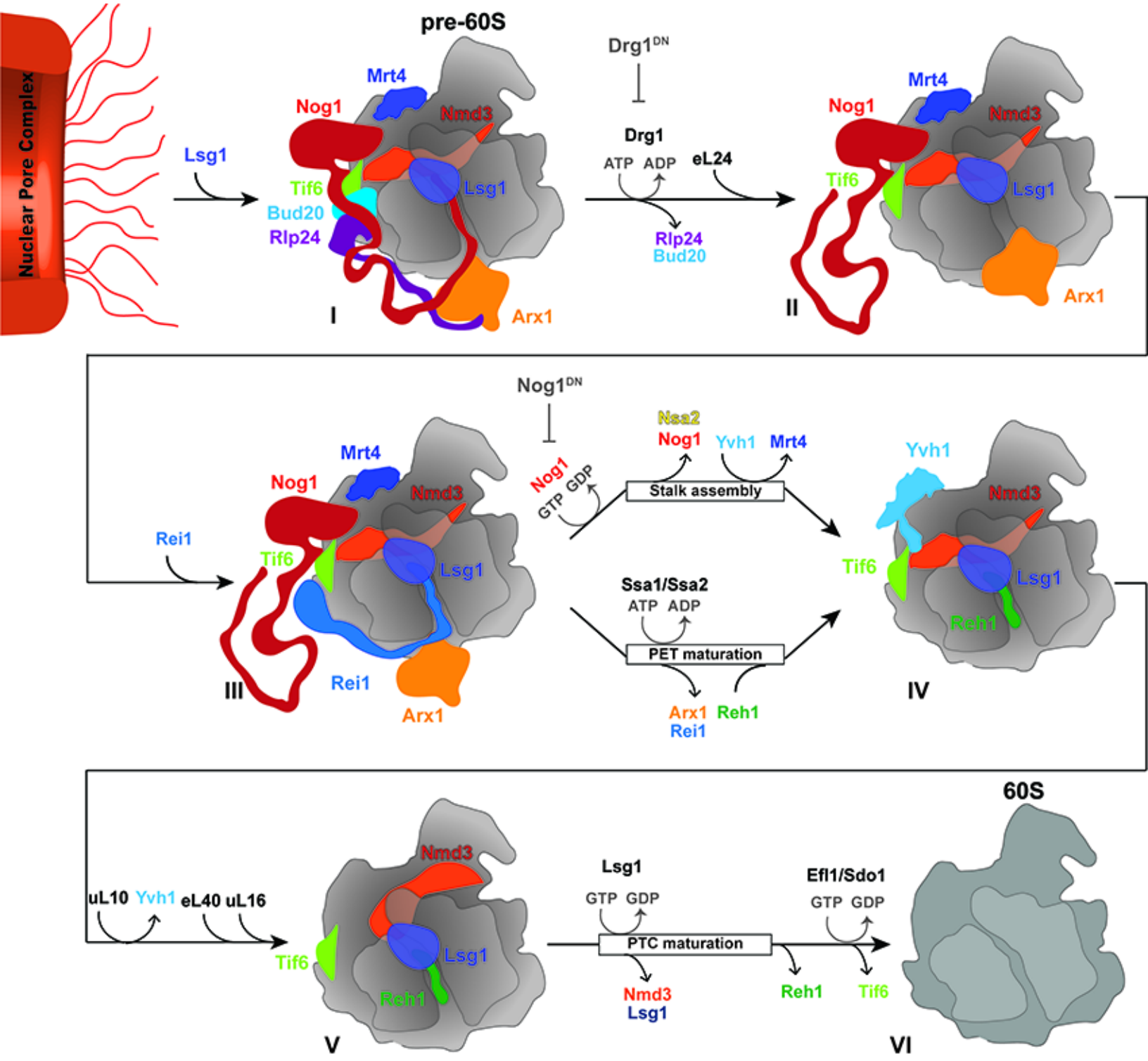
Nuclear Pore Complex
pre-60S
Lsg1
Mrt4
Nog1
Nmd3
Tif6
Bud20
Rlp24
Lsg1
Arx1
I
Drg1DN
Drg1
ATP ADP
eL24
Rlp24
Bud20
II
Nog1DN
Nog1
GTP GDP
Nsa2
Nog1
Yvh1
Mrt4
Stalk assembly
Rei1
III
Rei1
Ssa1/Ssa2
ATP ADP
PET maturation
Arx1
Rei1
Reh1
IV
Yvh1
Reh1
uL10 Yvh1 eL40 uL16
V
Lsg1
GTP GDP
PTC maturation
Nmd3
Lsg1
Efl1/Sdo1
GTP GDP
Reh1
Tif6
60S
VI

Figure 8